ARTICLES
https://doi.org/10.1038/s41592-020-0889-6

nature methods

Check for updates

Novel NanoLuc substrates enable bright two-population bioluminescence imaging in animals

Yichi Su[1,2,12], Joel R. Walker[3,12], Yunhee Park[1,2], Thomas P. Smith[3], Lan Xiang Liu[1,2], Mary P. Hall[4], Louai Labanieh[2], Robin Hurst[4], David C. Wang[1,5], Lance P. Encell[4], Namdoo Kim[1,2,6], Feijie Zhang[7,8], Mark A. Kay[7,8], Kerriann M. Casey[9], Robbie G. Majzner[7,10], Jennifer R. Cochran[2], Crystal L. Mackall[7,11], Thomas A. Kirkland[3] ✉ and Michael Z. Lin[1,2,7] ✉

Sensitive detection of two biological events in vivo has long been a goal in bioluminescence imaging. Antares, a fusion of the luciferase NanoLuc to the orange fluorescent protein CyOFP, has emerged as a bright bioluminescent reporter with orthogonal substrate specificity to firefly luciferase (FLuc) and its derivatives such as AkaLuc. However, the brightness of Antares in mice is limited by the poor solubility and bioavailability of the NanoLuc substrate furimazine. Here, we report a new substrate, hydrofurimazine, whose enhanced aqueous solubility allows delivery of higher doses to mice. In the liver, Antares with hydrofurimazine exhibited similar brightness to AkaLuc with its substrate AkaLumine. Further chemical exploration generated a second substrate, fluorofurimazine, with even higher brightness in vivo. We used Antares with fluorofurimazine to track tumor size and AkaLuc with AkaLumine to visualize CAR-T cells within the same mice, demonstrating the ability to perform two-population imaging with these two luciferase systems.

Bioluminescence imaging with luciferases is an essential technique for tracking cells and reporting biological events in preclinical animal models. Luciferases catalyze oxidation of chemical substrates to generate electronic excited states that then relax via photonic emission[1]. Because bioluminescence does not require excitation light, there is no autofluorescence produced during imaging and background is generated only by spontaneous substrate emission, which is negligible for commonly used substrates[1]. As a result, luciferase-based reporters achieve very high signal-to-background ratios, enabling noninvasive imaging of cells in deep tissues with lower limits of detection than fluorescence[2,3].

Since the first use of firefly luciferase (FLuc) and its substrate D-luciferin in mice more than two decades ago[4], researchers have attempted to develop brighter bioluminescent enzyme-substrate systems, with recent success. Aka luciferase (AkaLuc) and its substrate AkaLumine, derived from FLuc and D-luciferin, respectively, produce ~13 times more detectable light per reporter molecule from intrapulmonary locations[5]. Other improved bioluminescent systems are based on the highly catalytic blue-emitting luciferase NanoLuc, which uses furimazine (Fz) as its substrate[6]. In one case, the reporter Antares consists of two copies of the cyan-excitable orange fluorescent protein CyOFP1 fused to NanoLuc[7]. In another case, red enhanced nano-lantern consists of two copies of the orange fluorescent protein dTomato fused to NanoLuc[8]. In these proteins, Förster resonance energy transfer (RET) from the NanoLuc reaction product to CyOFP1 or dTomato shifts a large fraction of emission to wavelengths above 600 nm, which transmit through mammalian tissue more efficiently[9]. Antares has recently been further developed into Antares2, which uses diphenylterazine (DTZ), a furimazine derivative with red-shifted emission[7,10].

Further improvements to NanoLuc-based enzyme-substrate systems such as Antares-Fz would be of widespread use for two reasons. First, FLuc and NanoLuc are orthogonal in their substrate specificity, due to their unrelated structures and enzymatic mechanisms, and thus can be used to image two biological processes or cell populations in the same animals[11–13]. Improving NanoLuc substrates would allow reporters such as Antares to reach higher levels of in vivo sensitivity, which would be useful for dual bioluminescence imaging experiments with FLuc-based reporters, regardless of the relative brightness of the two systems. Second, unlike insect-derived luciferases such as FLuc and its derivatives, NanoLuc does not require ATP as a cofactor[14]. This uniquely allows for applications of NanoLuc-based systems in the extracellular space; for example, the detection of cell surface receptors by application of NanoLuc-fused ligands[15,16] or the detection of antigens with NanoLuc-conjugated antibodies[17].

We hypothesized that further enhancement of NanoLuc-based in vivo bioluminescence reporting should be possible. For example, furimazine is poorly soluble in aqueous solutions whereas D-luciferin can be dissolved to high concentrations in buffered saline. Thus, while D-luciferin is routinely administered by intraperitoneal (i.p.) injection at 150 mg kg^{-1} (13 µmol for a 25-g mouse) to reach

[1]Department of Neurobiology, Stanford University, Stanford, CA, USA. [2]Department of Bioengineering, Stanford University, Stanford, CA, USA. [3]Promega Biosciences LLC, San Luis Obispo, CA, USA. [4]Promega Corporation, Madison, WI, USA. [5]Department of Biology, Stanford University, Stanford, CA, USA. [6]Department of Chemistry, Kongju National University, Gongju, South Korea. [7]Department of Pediatrics, Stanford University, Stanford, CA, USA. [8]Department of Genetics, Stanford University, Stanford, CA, USA. [9]Department of Comparative Medicine, Stanford University, Stanford, CA, USA. [10]Stanford Cancer Institute, Stanford University, Stanford, CA, USA. [11]Department of Medicine, Stanford University, Stanford, CA, USA. [12]These authors contributed equally: Yichi Su, Joel R. Walker. ✉e-mail: thomas.kirkland@promega.com; mzlin@stanford.edu

concentrations that saturate FLuc[18], the poor aqueous solubility of furimazine limits maximum dosage to only 1.3 µmol in the previously published polyethylene glycol-300 (PEG-300)-based aqueous formulation[7], while a dosage of 0.25 mg kg^{-1} (0.016 µmol for a 25-g mouse) in PBS has been routinely administered[11]. Furthermore, lipophilic compounds bind to plasma proteins and concentrate within adipose tissues, increasing their volumes of distribution and lowering their effective concentrations in extracellular fluid. Indeed, while Antares can produce >100-fold more photons than FLuc in cells incubated with saturating concentrations of substrates, its advantage in vivo is reduced to roughly threefold of FLuc due to the limited amount of furimazine that can be administered[7,10]. Thus, improving the solubility of furimazine could increase the sensitivity of NanoLuc-based bioluminescence imaging in animals.

Here, we report the development of new NanoLuc substrates with greater solubility and higher maximum possible doses in vivo. When administered by i.p. injection, the new substrates produced an approximately four- to fivefold improvement in Antares brightness from deep-tissue locations compared to furimazine at maximal doses. Antares with the new substrates also exhibits comparable performance to AkaLuc with AkaLumine for deep-tissue imaging in live mice. We name the two most optimal new substrates hydrofurimazine (HFz) and fluorofurimazine (FFz). Compared to furimazine, photon generation from HFz in vivo is both more intense and more prolonged, allowing Antares-based reporters to track dynamic events in vivo at high temporal resolution and for extended periods of time. FFz exhibits even higher peak and integrated brightness than HFz in vivo. We demonstrate that Antares with FFz and AkaLuc with AkaLumine can be used in the same subjects for dual bioluminescence imaging.

Results

As the brightness of in vivo NanoLuc-based reporters such as Antares is likely constrained by the maximum injectable amount of substrate, we set out to create NanoLuc substrates with improved solubility. NanoLuc is derived from *Oplophorus gracilis* luciferase, which uses coelenterazine as its natural substrate, as characterized by Shimomura[19]. Coelenterazine features a phenol group at the C6 position of the central imidazopyrazinone ring, whereas furimazine and DTZ contain the more hydrophobic phenyl group. We found furimazine to be more soluble than DTZ in the PEG-300-based aqueous formulation[7], so we selected furimazine as a starting point for synthesizing new substrates with improved solubility. Specifically, we synthesized derivatives of furimazine with polar substituents on the phenyl ring (Supplementary Fig. 1), creating a 4′-hydroxy substituent (designated compound A), a 3′-hydroxy substituent (compound B) and a 3′-amino substituent (compound C) (Fig. 1a and Supplementary Figs. 2–4). These compounds were indeed more soluble than furimazine (Extended Data Fig. 1a), reaching at least 8.8 versus 2.8 mM for furimazine in the PEG-300-based formulation. Compound B was noticeably more soluble than compounds A and C, dissolving well at a concentration of 28 mM.

We next characterized the new compounds as substrates for Antares. The emission spectrum of Antares, which comprises two peaks representing photons from the reaction product and post-RET emission from CyOFP1, were not substantially altered with the new substrates (Extended Data Fig. 1b). This finding indicates that the new substrates emitted with similar wavelength distributions as furimazine and, since donor quantum yield affects RET efficiency, that quantum yields of NanoLuc with the new substrates are also not substantially changed. Substrate titration assays revealed that compound B has similar V_{max} and thereby k_{cat} and higher k_{cat}/K_M compared to furimazine (Extended Data Fig. 1c). Light output decreased more rapidly over time with compound A than with the other substrates (Extended Data Fig. 1d), which suggests specific inhibition of NanoLuc by the product of compound A oxidation. Compared to furimazine, the new substrates also showed improved stability in serum (Extended Data Fig. 1e), a desirable characteristic for use in mice.

To facilitate comparisons between substrates or between bioluminescent reporters in mice, we constructed an Antares gene whose transcription from a constitutive promoter was dependent on Cre recombinase. This gene was integrated into the *H11* safe-harbor locus by φC31-mediated integration into an attP site previously inserted in that locus[20]. We could then introduce tissue-specific Cre drivers through genetic crosses. This experimental design reduces the number of experimental variables during comparisons between substrates, as reporters are driven by identical genetic elements and are expressed in a stable long-term manner.

To compare new substrates and furimazine brightness in deep tissues, we first expressed Antares in the liver by creating mice doubly hemizygous for an *albumin-Cre* gene and the *CAG-LSL-Antares*. We then administered 1.3 µmol of each substrate by i.p. injection in the previously used vehicle, which uses PEG-300 as the primary solubilizing agent[7]. We observed that peak light production was highest with compound B, followed by compound C and then compound A or furimazine, with the latter two demonstrating similar peak light levels (Fig. 1b). All three new substrates exhibited a slower onset to peak and clearly prolonged duration of bioluminescence compared to furimazine. Consequently, compound A produced more total integrated output even though its peak output was similar to that of furimazine (Fig. 1c). As the new substrates yield more signal in vivo despite performing similarly to or worse than furimazine in vitro, these results suggest the improved output is due to differences in bioavailability.

We next quantified light production in mice from Antares with the two most soluble substrates, compounds B and C. The maximum amount of compound C that could be administered i.p. in the PEG-300 formulation was 4.2 µmol due to an injection volume limit of ~0.5 ml, whereas it was possible to inject up to 13.3 µmol of compound B because of its higher solubility (Extended Data Fig. 1a). Here, 13.3 µmol of compound B produced similar brightness as 4.2 µmol (Extended Data Fig. 2a,b), establishing 4.2 µmol as a saturating dose for compound B. Specifically, compound B at saturating dose produced approximately fourfold more light than the maximum dose of furimazine. To further validate the performance of the new substrates in vivo, we performed a second set of imaging experiments in transgenic mice expressing Antares in the kidney using nestin-Cre/CAG-LSL-Antares mice, as nestin is known to be expressed during kidney development. These experiments confirmed that injecting higher amounts of the new substrates improved light production over furimazine (Extended Data Fig. 2c–f).

Given its high brightness and aqueous solubility, we selected compound B, which we named hydrofurimazine (HFz), for further characterization in vivo. AkaLuc-AkaLumine, Antares2-DTZ and LumiScarlet-8pyDTZ are other recently developed luciferase–luciferin pairs with in vivo performance superior to FLuc with D-luciferin. To assess how well Antares-HFz performs in vivo relative to these bioluminescent systems, we expressed Antares, Antares2, LumiScarlet or AkaLuc in nude mice by hydrodynamic transfection of plasmid DNA. After 18 h, the mice were injected i.p. with optimal doses of substrates and imaged (Fig. 2a,b and Extended Data Fig. 3). Specifically, we injected 4.2 µmol of HFz, the maximum soluble doses of DTZ and 8pyDTZ (1 and 4 µmol)[21] and the recommended dose of AkaLumine for AkaLuc (3 µmol)[5]. Time-lapse imaging revealed that all luciferase–substrate pairs were similar in peak intensity (Fig. 2b,c). Thus, the increased light production from Antares conferred by HFz allows NanoLuc-based bioluminescence systems to match that of the orthogonal AkaLuc-AkaLumine system. Antares-HFz also exhibited uniquely sustained emission (Fig. 2b,d), allowing its integrated signal over 20 min to significantly exceed that of Antares2-DTZ

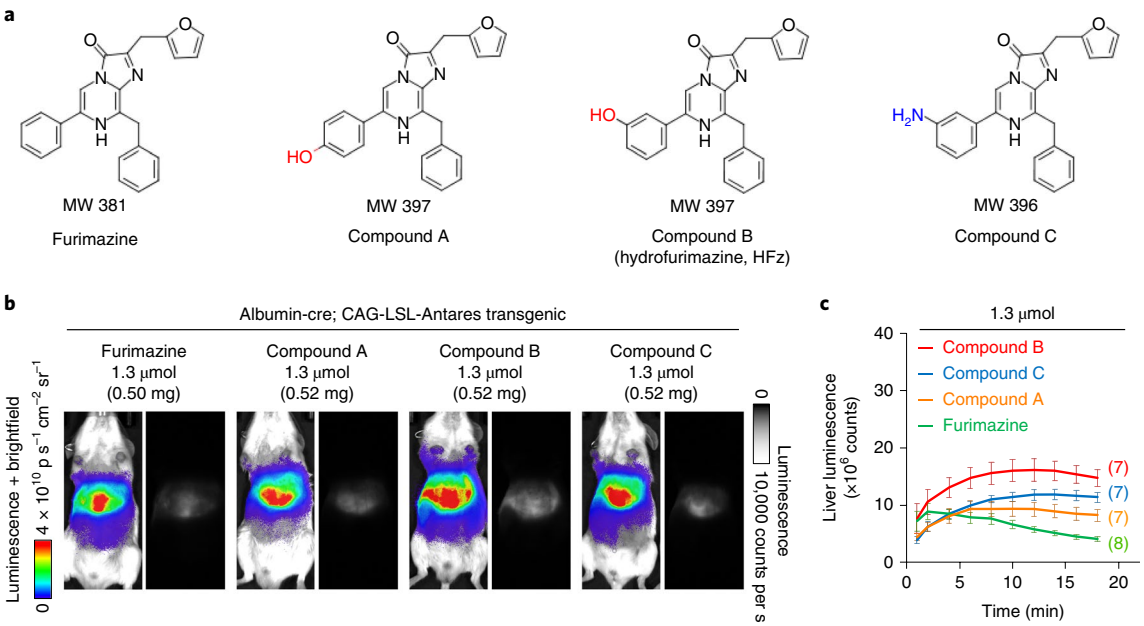

Fig. 1 | In vivo screening of new furimazine analogs. a, Structures of bioluminescent substrates. MW, molecular weight. **b**, Bioluminescence images of mice doubly hemizygous for *albumin-Cre* and *CAG-loxP-stop-loxP-Antares* (*CAG-LSL-Antares*) genes, which express Antares protein in the liver. Representative results with peak bioluminescence from each substrate injection were shown in two images. Left, linear pseudocolored representations of bioluminescence intensity overlaid on bright-field images, which is the more commonly used display format for bioluminescence in animals. Right, raw grayscale images, allowing intuitive assessment of relative brightness and visualization of anatomical features. This display format, while standard for fluorescence imaging, is rarely used for bioluminescence in animals. Exposure 1 s, binning 1, f-stop 8. **c**, Mean bioluminescence intensity over time for each amount of injected substrate. Error bars show s.e.m. Numbers of mice are indicated in parentheses.

(Fig. 2e). Integrated signal over 20 min also appeared higher than that of LumiScarlet-8pyDTZ, but narrowly missed statistical significance after adjusting for multiple comparisons (Fig. 2b,e). A difference in integrated signal may be more apparent with longer integration times.

Although HFz already demonstrates slower signal decay in vivo compared to previous substrates, further prolonging light production would be useful for time-lapse imaging of dynamic bioluminescent reporters. Aqueous solutions of poloxamer-407 (P-407) are liquid at room temperature but gel at body temperature, and can be used to create extended-release i.p. formulations of small-molecule drugs[22]. Conveniently, mice can be given P-407 for months (12 mg i.p. every 3 d) without affecting body weight, morbidity or mortality[23]. We found that after solubilizing 4.2 μmol (1.7 mg) of substrate with 12 mg P-407 in ethanol and evaporating the ethanol, the lyophilized cakes of P-407 with HFz, but not furimazine or compound C, could be resolubilized with 0.48 ml of water (Extended Data Fig. 4a). Mice injected daily for 3 d with this aqueous solution of HFz and P-407, or P-407 alone, were similar to uninjected mice in body weight or complete blood counts (Supplementary Table 1). On a comprehensive metabolic panel, the only consistent abnormality compared to uninjected controls was hypercholesterolemia (Supplementary Table 1), a previously described effect of P-407 that reverses on discontinuation[23]. In addition, no abnormalities were found on gross examination of organs or on histology of the liver, lung and kidney (Extended Data Fig. 4b).

We compared the P-407 formulation of HFz with the earlier PEG-300-based formulation for signal intensity and duration in mice. On i.p. administration to mice expressing Antares in the liver, the two formulations produced similar peak brightness, but light output with the P-407-based formulation peaked later and appeared more sustained (Extended Data Fig. 4c,d). Thus P-407, in addition to allowing lyophilization and water-reconstitution of HFz, also conferred sustained-release kinetics for NanoLuc-based bioluminescence imaging in vivo without sacrificing peak brightness.

This sustained-release formulation of HFz should be useful for bioluminescence imaging of physiological events in vivo over long time courses. To determine whether this is the case, we performed extended imaging of the Antares-based, orange-emitting, calcium-modulated bioluminescent indicator (Orange CaMBI) in mouse liver. Orange CaMBI has been used to noninvasively report calcium oscillations in the liver, but previous imaging sessions using furimazine were limited to 6 min in duration[24]. Using sustained-release HFz, orange CaMBI signals were sufficiently bright to be seen by the naked eye in the dark for >1 h and allowed time-lapse imaging with <1 s exposures using a consumer-grade digital camera. We observed Orange CaMBI reaching peak brightness 24 min after substrate injection, dropping to half of its peak brightness ~60 min after injection with monoexponential kinetics. Vasopressin administration was followed by oscillations in Orange CaMBI signals within liver regions with periods of ~45 s over a 45-min window (Fig. 2g), confirming previous results using furimazine over shorter time frames[24]. The combination of brightness and signal duration produced by HFz allowed calcium oscillations to be visualized with fine temporal resolution for >1 h after substrate injection (Fig. 2f). Thus, extended-release HFz enables bioluminescence imaging in vivo over long time courses, which should be useful for studying dynamic physiological events in real time.

As demonstrated by HFz and compound C, improving solubility and bioavailability is a promising strategy for engineering new substrates derived from furimazine. We next explored other strategies to further improve their in vivo performance. In medicinal chemistry, fluorination on a target molecule is often adopted in drug design to alter potency, membrane permeability, metabolism and pharmacokinetics properties[25]. We thus synthesized derivatives of HFz and compound C with fluorine substitution on the phenyl ring (Supplementary Fig. 1), creating two new substrates with 2′-fluoro substituents (designated compound D and E) (Fig. 3a and Supplementary Figs. 5 and 6). In vitro, these fluorinated

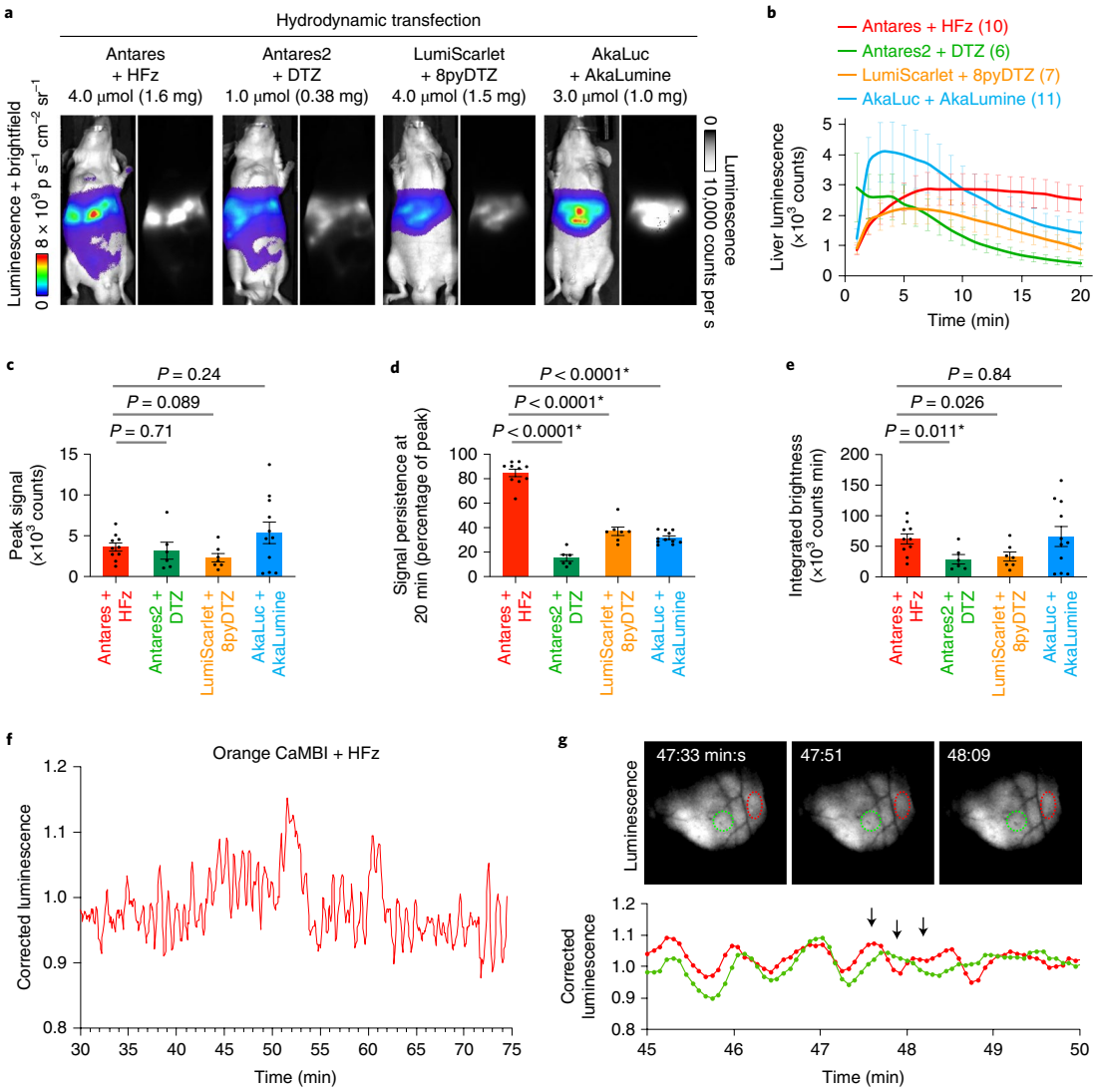

Fig. 2 | In vivo characterization and application of compound B (HFz). a, Representative results of bioluminescence imaging in J:NU mice hydrodynamically transfected with plasmids encoding Antares, Antares2, LumiScarlet or AkaLuc. Maximal amounts of corresponding luciferins were injected i.p. Images from the time point of maximal brightness are displayed with the same intensity scaling. Exposure 1 s, binning 1, f-stop 1.2. **b**, Mean signal intensity in the liver over time for luciferase–luciferin systems. Error bars show s.e.m. Numbers of mice are indicated in parentheses. **c**, Mean peak signal intensities of the three systems, calculated from the peak intensities of individual mice. **d**, Signal persistence, quantified in each mouse as intensity at 20 min divided by peak intensity. **e**, Total integrated signal, quantified from the sum of signals from 0 to 20 min for individual mice. **c–e**, Error bars show s.e.m. *P* values, two-tailed Welch's unpaired *t*-test. Asterisks, statistically significant differences indicated by *P* values below 0.0167 (for an overall alpha level of 0.05 for three comparisons by the Bonferroni method). **f**, Bioluminescence imaging of calcium in mouse liver with Orange CaMBI and extended-release compound B (HFz). Emission from Orange CaMBI in one region of the liver reveals calcium oscillations. Raw luminescence was corrected for substrate decay by fitting to a monoexponential decay curve. **g**, Top, bioluminescence images at three time points showing localized changes in CaMBI activity. Below, bioluminescence intensity within two regions as indicated in the bioluminescence images. Arrows indicate the time points corresponding to the three images. Results in **f** and **g** were repeated independently twice with similar results.

compounds do not alter the emission spectrum of Antares (Extended Data Fig. 5a), while exhibiting improved V_{max} and thereby k_{cat} versus furimazine (Fig. 3a and Extended Data Fig. 5b), and retaining the improved stability in serum observed with HFz and compound C (Extended Data Fig. 5c). More importantly, when 1.3 µmol of each substrate in the PEG-300 formulation was administered by i.p. injection, both compound D and E showed brighter signal outputs than HFz in mouse liver. Compound E in particular showed an approximately threefold improvement (Fig. 3b,c). As compound E yields greater improvement in vivo than in vitro, these results suggest the improved light output is likely due to differences in both enzyme use and bioavailability brought by fluorination.

Encouraged by the improved performance of singly fluorinated compounds over their nonfluorinated analogs and by the brighter signal of compound E over compound D, we introduced another fluorine substitution on a different phenyl ring of compound E, leading to compound F (Supplementary Fig. 7 and Fig. 3a). Compared to compound E, compound F displays a higher V_{max} and thereby k_{cat} for Antares in vitro and a further increase in peak signal when administered at 1.3 µmol in vivo (Fig. 3b,c and Extended Data Fig. 5a–c). We then characterized the solubility of compounds E and F, finding them to be as soluble as the parent compound C, reaching at least 8.8 mM in the PEG-300-based formulation (Extended Data Fig. 5d). Compound F was especially

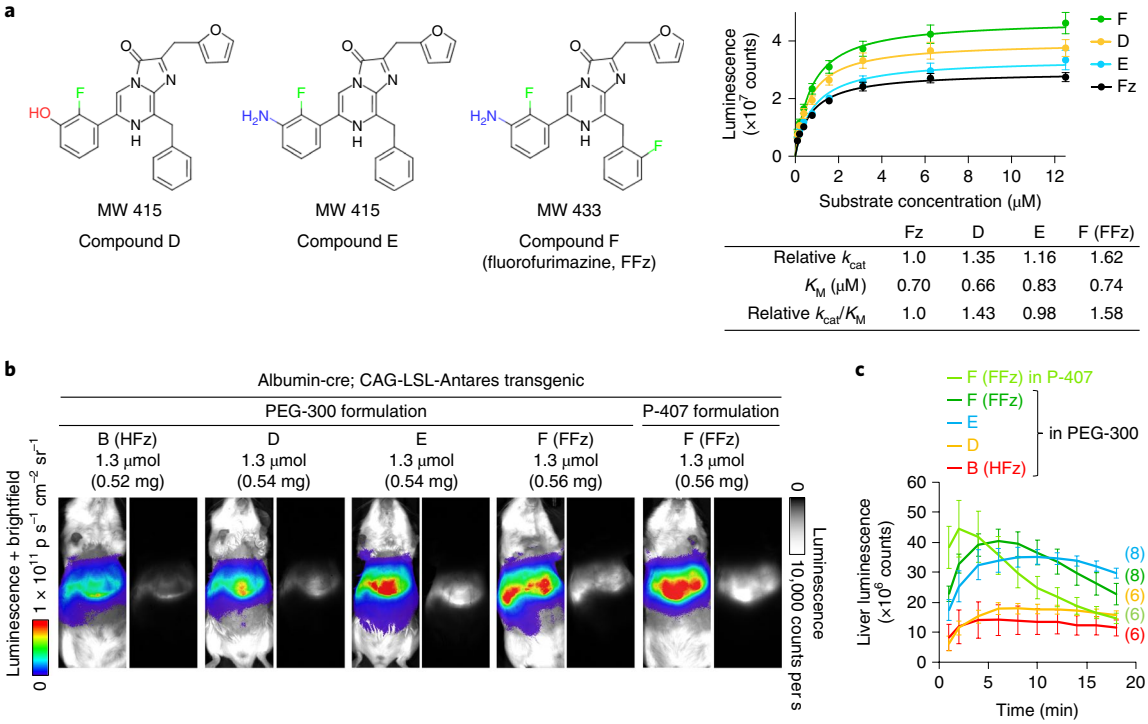

Fig. 3 | In vitro characterization and in vivo screening of new fluorinated furimazine analogs. a, Left, structures of fluorinated furimazine analogs. Right, determination of kinetic parameters of relative k_{cat} and absolute K_M for Antares with each substrate. As the same concentration of purified Antares was used with each substrate, k_{cat} relative to furimazine can be calculated from the relative asymptotic luminescence (V_{max}) values. Center values, mean. Error bars show s.e.m. $N = 3$ independent experiments. **b**, Bioluminescence imaging results in mice doubly hemizygous for *albumin-Cre* and *CAG-loxP-stop-loxP-Antares* (*CAG-LSL-Antares*) genes, which express Antares protein in the liver, at 6–8 weeks of age and injected with indicated amount of fluorinated furimazine analogs. Representative results with peak bioluminescence were shown in two images, with conditions of experiments and data processing same as that of Fig. 1b. Exposure 1 s, binning 1, f-stop 8. **c**, Mean bioluminescence intensity over time for each amount of injected substrate. Error bars show s.e.m. Numbers of mice are indicated in parentheses.

soluble in the P-407 formulation, dissolving well at a concentration of 8.8 mM, while compound E and C could not be solubilized at this concentration. Unexpectedly, however, compound F displayed a shorter in vivo bioluminescence half-life in the P-407 than PEG-300 formulation. Regardless, as compound F produced the most light per mole both in vitro and in vivo, and was the most soluble fluorinated compound, we named it fluorofurimazine (FFz) and selected it for further characterization.

We first established the optimal dosage and vehicle for FFz administration in mice. An injection of 1.3 μmol FFz produced more light from the mouse liver than 4.2 μmol HFz (Extended Data Fig. 6a,b), while requiring a smaller injection volume of only 0.15 ml compared to 0.48 ml. No abnormalities in body weight, blood chemistry or histology were found in mice injected with 1.3 μmol FFz in P-407 daily for 3 d. A dose of 4.2 μmol of FFz produced more light than 1.3 μmol (Extended Data Fig. 6b), but was associated with weight loss, abnormal blood chemistry (Supplementary Table 2) and histologic evidence of kidney toxicity and hepatic subcapsular degeneration (Extended Data Fig. 6c and Supplementary Table 3). These results indicate that FFz can be safely administered at a dose of 1.3 μmol in P-407, at which it produces more light than 4.2 μmol HFz in mice.

As lack of spontaneous emission by substrates is crucial for the high signal-to-background ratio of bioluminescence imaging, we directly tested the level of spontaneous emission from furimazine, HFz or FFz in vivo. We injected each substrate into wild-type mice not expressing any reporter, allowing us to assess true background in the known absence of enzyme. All tested NanoLuc substrates, including furimazine, HFz and FFz and FLuc substrate D-luciferin, produced negligible signals after injection under sensitive imaging settings, while AkaLumine produced clear background signal in the liver (Fig. 4a and Extended Data Fig. 7a,b).

We next assessed how well Antares with FFz compared to AkaLuc with AkaLumine. In hydrodynamic transfection experiments, Antares with 1.3-μmol FFz tended to produce more brightness than AkaLuc with AkaLumine, although the effect was not statistically significant with the observed variance and the number of mice tested (Fig. 4b–d and Extended Data Fig. 7c). Kinetics of light production were similar between these two systems (Fig. 4c). To more tightly correlate expression between Antares and AkaLuc, we also created HeLa cells stably expressing both proteins from a bicistronic gene using a P2A sequence, thereby translating the same number of messenger RNA molecules. In cells, the ratio of AkaLuc signal over Antares signal was higher in HeLa(Antares-P2A-AkaLuc) cells than in HeLa(AkaLuc-P2A-Antares), unexpectedly (Fig. 4e). We thus selected HeLa(Antares-P2A-AkaLuc) cells for in vivo experiments to obtain as much signal from AkaLuc as possible. After implanting 1,000 cells subcutaneously in the left thoracolumbar region, we imaged mice using FFz and AkaLumine sequentially (Fig. 4f). Half the mice were imaged first with FFz and then, after signals decayed, with AkaLumine, while the other mice were imaged in the reverse order. As the order of injection did not noticeably affect results, samples were combined for analysis. Antares with FFz exhibited threefold more bioluminescence than AkaLuc with AkaLumine, quantified as either peak intensity or integrated signal (Fig. 4g and Extended Data Fig. 7d). AkaLumine-injected mice exhibited substantial bioluminescence from the upper abdomen (Fig. 4f), consistent with the background liver signal observed in mice injected

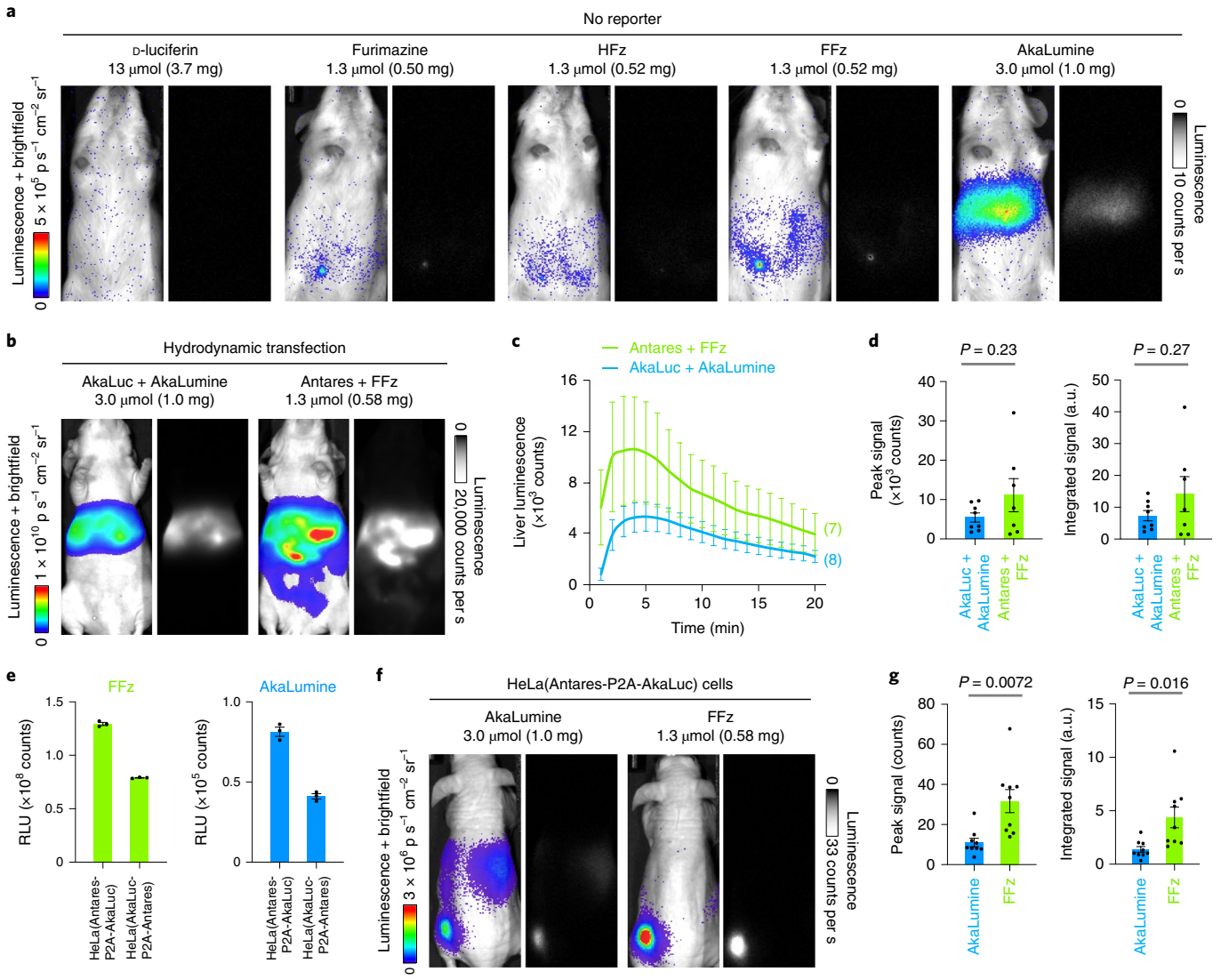

Fig. 4 | In vivo characterization and application of FFz. a, Background luminescence for the new substrates, D-luciferin and AkaLumine in unshaved white fur coated mice. The experiment was repeated independently twice with similar results. **b**, Representative results of bioluminescence imaging in J:NU nude mice hydrodynamically transfected with plasmids encoding Antares or AkaLuc. Maximal amounts of corresponding luciferins were injected i.p. Images in each type are displayed with the same intensity scaling and represent the time point of maximal brightness. Exposure 1 s, binning 1, f-stop 1.2. **c**, Mean signal intensity in the liver over time for luciferase–luciferin systems. Error bars show s.e.m. Numbers of mice are indicated in parentheses. **d**, Left, mean peak signal intensities of each system. Right, Total integrated signal, quantified from the sum of signals from 0 to 20 min for individual mice. Error bar show s.e.m., *P* values, two-tailed Welch's *t*-test. **e**, In vitro assay of expression of luciferase in transgenic HeLa cell lines. $N = 3$. **f**, Representative results of bioluminescence imaging in J:NU nude mice subcutaneously implanted with 10^3 HeLa cells stably expressing both Antares and AkaLuc luciferases. Exposure 60 s, binning 2, f-stop 1.2. **g**, Left, mean peak signal intensities. Right, total integrated signal, quantified from the sum of signals from 0 to 20 min for individual mice. $N = 9$. Error bars show s.e.m. *P* values, two-sided Welch's unpaired *t*-test.

with AkaLumine in the absence of AkaLuc expression (Fig. 4a and Extended Data Fig. 7b).

Luciferases are commonly used to track the location and growth of tumors in mice. We thus tested the ability of Antares and AkaLuc to report the growth of engrafted EW8 Ewing sarcoma cells in nod scid mice. We transfected EW8 cells with plasmids expressing Antares or AkaLuc-P2A-CyOFP, where the CyOFP allowed us to ascertain how similarly the two luciferases were expressed. Despite Antares containing two copies of CyOFP, we observed similar brightness distributions in the CyOFP channel for the stably expressing population (Extended Data Fig. 8a), indicating the AkaLuc-P2A-CyOFP mRNA was translated as well or better than the Antares mRNA. We then selected for high stable expression of both luciferases using the same range of CyOFP values, and created xenografts in nod scid mice (Extended Data Fig. 8a–c). Unexpectedly, the EW8(Antares) tumors produced >100-fold more signal after FFz injection than the EW8(AkaLuc) tumors did after AkaLumine infection (Extended Data Fig. 8b,c). In addition, the EW8(Antares) tumors exhibited increasing bioluminescence over 6 d in six of the nine mice imaged, whereas EW8(AkaLuc) tumors showed a drop in signal in all the mice imaged (Extended Data Fig. 8b,c). We also observed decreasing bioluminescence over time from engrafted MG63.3 osteosarcoma cells stably expressing AkaLuc in nod scid gamma (NSG) mice administered native T cells (Extended Data Fig. 9a–d). The reasons for decreasing AkaLuc signals are unclear, but they could indicate effects of AkaLuc on long-term cell viability, decreasing AkaLuc expression or decreasing access of AkaLumine to the tumor cells due to stroma formation.

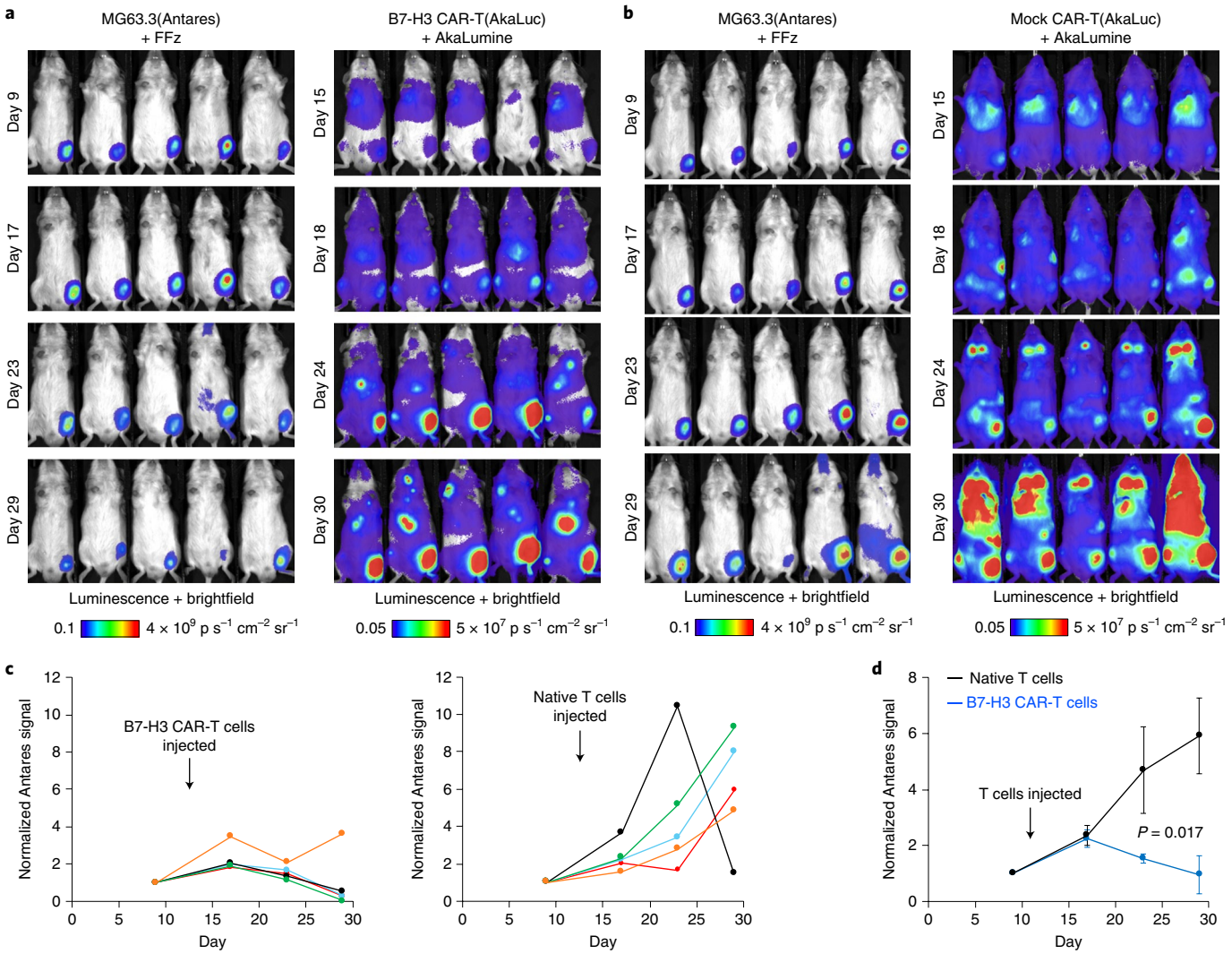

Fig. 5 | Dual bioluminescence imaging of tumor xenografts and CAR-T cells in vivo. a,**b**, Bioluminescence imaging in NSG mice engrafted with Antares-expressing MG63.3 tumors in one leg (at day 0) and intravenously injected with AkaLuc-expressing B7-H3 CAR-T cells (**a**) or native T cells (**b**) (at day 14). Maximal amounts of individual luciferins were injected i.p. on the indicated days. **c**, Normalized intensities of individual mice. **d**, Mean signal intensity of tumor over time, normalized to day 9 posttumor cell injection (first time point). $N = 5$. Error bars show s.e.m. P value, two-tailed Welch's unpaired t-test.

The ability to image distributions of cancer cells and immune cells in the same subjects would be extremely useful in mouse models of immunotherapy. Changes in tumor size and changes in immune cell number and distribution can then be visualized in the same subjects, providing clearer evidence for immune-mediated effects than imaging of either cell type alone. Moreover, sensitive reporters could shed light on dynamic responses of immune cells such as proliferation and trafficking. In mice bearing Antares-expressing MG63.3 cells (Extended Data Fig. 10a,b), we administered either native T cells expressing AkaLuc or T cells coexpressing AkaLuc and B7-H3 CAR, which targets MG63.3 cells. Bioluminescence from the Antares-expressing MG63.3 tumors increased over time in mice treated with the native T cells (Fig. 5b and Extended Data Fig. 10d) as expected, unlike the decreasing signals we had observed from AkaLuc-expressing MG63.3 tumors. In contrast, bioluminescence from the Antares-expressing MG63.3 tumors in mice treated with the AkaLuc- and CAR-expressing T cells decreased 9 d following T cell administration (Fig. 5a and Extended Data Fig. 10c). This resulted in significantly lower Antares signals in mice treated with CAR-T cells than mice treated with native T cells (Fig. 5c,d), confirming that tumor regression was CAR-mediated. AkaLuc imaging revealed both native and CAR-expressing T cells to colocalize with the tumor (Fig. 5a,b and Extended Data Fig. 10c,d), suggesting that specific antigen recognition, and not simply T cell presence in the tumor, is required for an antitumor effect. Taken together, these results establish the ability of Antares and AkaLuc to be used for orthogonal imaging of two cell populations in vivo, and demonstrate how dual luciferase imaging can be used to reveal the relationship between T cell distributions and tumor responses within individual mice.

Discussion

In this study, we developed new substrates for NanoLuc-based bioluminescent reporters that are more water-soluble than furimazine. We demonstrate that these new substrates improve the effective brightness of the NanoLuc-based Antares reporter in vivo. One specific substrate, HFz, can be dosed to saturating concentrations by simple i.p. injections. Antares with HFz produces fourfold higher brightness than a saturating dose of furimazine in Antares-expressing transgenic mice, and displays comparable brightness and superior

signal duration than AkaLuc with AkaLumine or Antares2 with DTZ. We created a formulation for HFz that allows dry storage and rapid reconstitution with water, demonstrates low toxicity in mice and exhibits extended-release properties in vivo. With this extended-release formulation, Antares produced a highly persistent signal with half-life of >30 min. The intensity and duration of this signal allowed for noninvasive visualization of calcium oscillations in the liver with high temporal resolution for over 1 h. Another substrate, FFz, displays even higher molar brightness than HFz, allowing lower i.p. injection volume for long-term studies. Antares with FFz at optimal dose produces threefold higher brightness than AkaLuc with AkaLumine in a cell implantation mouse model. Together with the orthogonal AkaLuc system, Antares with FFz enabled imaging distributions of cancer cells and immune cells in the same subjects in mouse models of immunotherapy. Thus, Antares with extended-release HFz will be especially useful in experiments visualizing dynamic events over time, while FFz will be most useful for detecting small numbers of cells.

Our results demonstrate the importance of substrate solubility and bioavailability as practical limitations to bioluminescence imaging in vivo. We found that introducing a hydrophilic entity (hydroxy- or amino-) onto the phenyl group of furimazine resulted in improved substrate solubility and bioavailability while preserving use by NanoLuc. Antares with the resulting substrate, HFz, produced similar peak and integrated bioluminescence as AkaLuc with AkaLumine on i.p. injection. As demonstrated by FFz, fluorination of the phenyl and benzyl rings further improves in vivo brightness. While FFz produces approximately threefold more photons per mole than HFz in mice, it is only 1.1-fold brighter in vitro, suggesting the in vivo improvement is due to better bioavailability.

Our study also demonstrates how transgenic expression of reporters enables rapid substrate screening. The coefficient of variation in measurements of HFz brightness was lower when Antares was expressed in the liver by transgenesis (~30%) than when it was expressed by hydrodynamic transfection (~71% over all injections). As the route of substrate administration was the same in both sets of mice, this demonstrates that variability in reporter expression after hydrodynamic transfection dominates over variability in substrate supply by i.p. injection. This is not surprising, as the process of hydrodynamic injection is inherently variable due to differences in vascular volume and structure between mice[26] and sensitive to trial-to-trial differences in the difficult tail vein injection procedure. Stable expression from the same genomic locus eliminates these sources of variability present in transient transfection, and thus allows for rapid testing of different substrates with smaller numbers of mice. We note, however, that our results in transgenic mice may have underestimated the per-molecule performance of Antares versus FLuc due to lack of complementary DNA optimization. FLuc was encoded by the *Luc2* gene with cryptic transcription factor sites removed and codon usage optimized for mammalian expression, which produces four- to 12-fold more FLuc in mammalian cells than the nonoptimized synonymous *Luc*$^{+}$ gene[27]. In contrast, the *Antares* gene has not undergone any coding sequence optimization. In addition, the *Luc2* gene was preceded by a Kozak sequence whereas the *Antares* gene was not. In the future, similar optimizations to the *Antares* gene could be introduced for a fairer comparison.

Whether furimazine-like substrates show spontaneous light production in vivo has recently been questioned[5]. Our results conclusively demonstrate that Antares substrates on their own do not spontaneously produce light in vivo. Our testing method was to simply inject substrates into mice not expressing any luciferase. This straightforward approach had also been used to demonstrate minimal spontaneous emission from DTZ in vivo[10]. However, some confusion has arisen from observations that injection of Antares2-expressing cells followed by DTZ produced widespread luminescence throughout the body, while injection of AkaLuc-expressing cells followed by AkaLumine produced luminescence at only defined sites[5]. A recent study has provided a clear explanation for these findings[28]. When Antares2-expressing cells are injected, dying cells release active Antares2 into the bloodstream, which is active because Antares2 does not require any cofactors to catalyze oxidation of its substrates. Thus, testing for spontaneous light production from furimazine-related substrates should be performed by injecting substrates into mice that do not express a NanoLuc-based reporter anywhere in the body. In contrast, because AkaLuc requires ATP, which is absent in blood, and because AkaLuc is also inactivated by plasma proteins, lysis of AkaLuc-expressing cells does not result in bioluminescence from the bloodstream. This difference in ATP dependence between luciferases should be considered when designing experiments.

Our results suggest several avenues for future exploration. First, the performance of furimazine analogs for bioluminescence reporting in the brain would be interesting to investigate. In preliminary work, we have observed that Antares with our newly reported furimazine derivatives is as bright or brighter in the brain than FLuc with luciferin. Second, the brightness of NanoLuc-based systems in animals could be further improved. As demonstrated by the development of AkaLuc or Antares2, NanoLuc could be evolved to improve its use of new substrates. In particular, higher brightness is possible if the NanoLuc domain within Antares can be evolved to catalyze light production from HFz or FFz with faster kinetics or higher quantum yield. Alternatively, effective brightness in mammals can be improved by increasing the fraction of total emission above 600 nm, which is currently only ~50% for Antares with HFz or FFz. Substituting a RET acceptor for NanoLuc with emission more red-shifted than CyOFP1 could thus further improve brightness in vivo.

In summary, HFz and FFz enable sensitive bioluminescence imaging for either prolonged light production of high sensitivity. Notably, existing NanoLuc-based reporters, including those in cell lines and transgenic mice, can benefit immediately these improved substrates without modification. Prolonged light production with HFz makes it the optimal substrate for dynamic reporters such as CaMBI, while the intensity of light production with FFz makes it well suited for tasks where sensitivity is important such as visualizing tumor growth, viral spread or gene expression. Finally, Antares with FFz and AkaLuc with AkaLumine enable imaging of two biological entities in the same animal subjects with similarly high sensitivity. By enabling experiments on the interactions between immune and cancer cells, as we have demonstrated here, or between immune cells and pathogens, dual bioluminescence imaging with high sensitivity is likely to have widespread use in biomedical research.

Online content

Any methods, additional references, Nature Research reporting summaries, source data, extended data, supplementary information, acknowledgements, peer review information; details of author contributions and competing interests; and statements of data and code availability are available at https://doi.org/10.1038/s41592-020-0889-6.

Received: 18 March 2019; Accepted: 8 June 2020;
Published online: 13 July 2020

References

1. Prescher, J. A. & Contag, C. H. Guided by the light: visualizing biomolecular processes in living animals with bioluminescence. *Curr. Opin. Chem. Biol.* **14**, 80–89 (2010).
2. Genevois, C., Loiseau, H. & Couillaud, F. In vivo follow-up of brain tumor growth via bioluminescence imaging and fluorescence tomography. *Int. J. Mol. Sci.* **17**, 1815 (2016).

3. Levin, R. A. et al. An optimized triple modality reporter for quantitative in vivo tumor imaging and therapy evaluation. *PLoS ONE* **9**, e97415 (2014).
4. Contag, C. H. et al. Visualizing gene expression in living mammals using a bioluminescent reporter. *Photochemistry Photobiol.* **66**, 523–531 (1997).
5. Iwano, S. et al. Single-cell bioluminescence imaging of deep tissue in freely moving animals. *Science* **359**, 935–939 (2018).
6. Hall, M. P. et al. Engineered luciferase reporter from a deep sea shrimp utilizing a novel imidazopyrazinone substrate. *ACS Chem. Biol.* **7**, 1848–1857 (2012).
7. Chu, J. et al. A bright cyan-excitable orange fluorescent protein facilitates dual-emission microscopy and enhances bioluminescence imaging in vivo. *Nat. Biotechnol.* **34**, 760 (2016).
8. Suzuki, K. et al. Five colour variants of bright luminescent protein for real-time multicolour bioimaging. *Nat. Commun.* **7**, 13718 (2016).
9. Zhao, H. et al. Emission spectra of bioluminescent reporters and interaction with mammalian tissue determine the sensitivity of detection in vivo. *J. Biomed. Opt.* **10**, 41210 (2005).
10. Yeh, H.-W. et al. Red-shifted luciferase–luciferin pairs for enhanced bioluminescence imaging. *Nat. Methods* **14**, 971 (2017).
11. Stacer, A. C. et al. NanoLuc reporter for dual luciferase imaging in living animals. *Mol. Imaging* **12**, 1–13 (2013).
12. Germain-Genevois, C., Garandeau, O. & Couillaud, F. Detection of brain tumors and systemic metastases using NanoLuc and Fluc for dual reporter imaging. *Mol. Imaging Biol.* **18**, 62–69 (2016).
13. Taylor, A., Sharkey, J., Plagge, A., Wilm, B. & Murray, P. Multicolour in vivo bioluminescence imaging using a NanoLuc-based BRET reporter in combination with firefly luciferase. *Contrast Media Mol. Imag.* **2018**, 2514796 (2018).
14. Mezzanotte, L., van 't Root, M., Karatas, H., Goun, E. A. & Löwik, C. W. G. M. In vivo molecular bioluminescence imaging: new tools and applications. *Trends Biotechnol.* **35**, 640–652 (2017).
15. England, C. G., Ehlerding, E. B. & Cai, W. NanoLuc: a small luciferase is brightening up the field of bioluminescence. *Bioconjug Chem.* **27**, 1175–1187 (2016).
16. Gopalakrishnan, R. et al. A novel luciferase-based assay for the detection of chimeric antigen receptors. *Sci. Rep.* **9**, 1957 (2019).
17. Nath, N., Flemming, R., Godat, B. & Urh, M. Development of NanoLuc bridging immunoassay for detection of anti-drug antibodies. *J. Immunol. Meth.* **450**, 17–26 (2017).
18. Edinger, M. et al. Noninvasive assessment of tumor cell proliferation in animal models. *Neoplasia* **1**, 303–310 (1999).
19. Inouye, S. & Shimomura, O. The use of renilla luciferase, oplophorus luciferase, and apoaequorin as bioluminescent reporter protein in the presence of coelenterazine analogues as substrate. *Biochem Biophys. Res. Commun.* **233**, 349–353 (1997).
20. Tasic, B. et al. Site-specific integrase-mediated transgenesis in mice via pronuclear injection. *Proc. Natl Acad. Sci. USA* **108**, 7902–7907 (2011).
21. Yeh, H. W. et al. ATP-independent bioluminescent reporter variants to improve in vivo imaging. *ACS Chem. Biol.* **14**, 959–965 (2019).
22. Bodratti, A. M. & Bodratti, P. Formulation of poloxamers for drug delivery. *J. Funct. Biomater.* **9**, 11 (2018).
23. Johnston, T. P. et al. Potential downregulation of HMG-CoA reductase after prolonged administration of P-407 in C57BL/6 mice. *J. Cardiovasc. Pharm.* **34**, 831–842 (1999).
24. Oh, Y. et al. An orange calcium-modulated bioluminescent indicator for non-invasive activity imaging. *Nat. Chem. Biol.* **15**, 433–436 (2019).
25. Gillis, E. P., Eastman, K. J., Hill, M. D., Donnelly, D. J. & Meanwell, N. A. Applications of fluorine in medicinal chemistry. *J. Med. Chem.* **58**, 8315–8359 (2015).
26. Suda, T. & Liu, D. Hydrodynamic gene delivery: its principles and applications. *Mol. Ther.* **15**, 2063–2069 (2007).
27. Mašek, T., Vopalenský, V. & Pospíšek, M. The Luc2 gene enhances reliability of bicistronic assays. *Open Life Sci.* **8**, 423–431 (2013).
28. Yeh, H. W., Wu, T., Chen, M. & Ai, H. W. Identification of factors complicating bioluminescence imaging. *Biochemistry* **58**, 1689–1697 (2019).

Methods

Synthetic procedures. In general, substrates were synthesized using organic synthetic methodology as previously described[29]. Specific reaction conditions and analytical results are described below.

***tert*-Butyl 2-diazo-2-(diethoxyphosphoryl)acetate (compound 2 in Supplementary Fig. 1).** To a solution of 4-methylbenzenesulfonyl azide (29.1 g, 147 mmol) in THF (300 ml) at 0 °C, sodium hydride was added (5.9 g, 147 mmol, 60% oil dispersion) in ~1-g batches. *Tert*-butyl 2-(diethoxyphosphoryl)acetate (31.0 g, 123 mmol) was added dropwise over 30 min. The mixture stirred for 1 h at 0 °C and 2 h at room temperature. A mixture of ether and ice water was prepared in 2-l beaker and the reaction mixture was carefully added with stirring. The two layers were separated and the aqueous layer was extracted with ether. The organic layers were combined, dried with sodium sulfate, filtered, concentrated and purified with silica gel chromatography in heptane and ethyl acetate to afford the desired product (32.9 g, 96%) as a yellow mobile oil. ^{1}H nuclear magnetic resonance (NMR) (400 MHz, $CDCl_3$) δ 4.32–4.09 (multiplet (m), 4H), 1.51 (singlet (s), 9H), 1.38 (triplet of doublets (td), coupling constant J = 7.1, 0.8 Hz, 6H); ^{13}C NMR (101 MHz, $CDCl_3$) δ 162.56 (doublet (d), J = 12.1 Hz), 128.06 (d, J = 323 Hz), 83.02, 63.44 (d, J = 5.7 Hz), 28.25, 16.17 (d, J = 6.9 Hz); high-performance liquid chromatography (HPLC) 99.3% (area under curve (AUC) at 254 nm) 5.03 min (Synergi Max-RP, water/ACN 0.1%TFA).

5-Bromo-3-(2-fluorobenzyl)pyrazin-2-amine (compound 4b). To an oven dried flask, acid activated zinc (10.4 g, 15 9 mmol) was suspended in THF (40 ml) at room temperature. Here, 1-(bromomethyl)-2-fluorobenzene (10.0 g, 52.9 mmol) was added and the suspension was heated to reflux for 1 h. The reaction was cooled to room temperature and the supernatant was transferred to a flask containing 3,5-dibromopyrazin-2-amine (6.1 g, 24.1 mmol), bis(triphenylphosphine) palladium(II) dichloride (0.84 g, 1.2 mmol) and THF (40 ml). The mixture was heated to 50 °C for 4 h. After cooling, the mixture was diluted with ethyl acetate and water. The two layers were separated and the aqueous layer was extracted with ethyl acetate. The organic layers were combined, dried with sodium sulfate, filtered, concentrated and purified with silica gel chromatography in heptane and ethyl acetate to afford desired product (3.0 g, 44%) as a light yellow solid. ^{1}H NMR (400 MHz, DMSO-d_6) δ 7.96 (s, 1H), 7.44–7.01 (m, 4H), 6.60 (s, 2H), 4.14 (s, 2H); ^{13}C NMR (101 MHz, DMSO-d_6) δ 162.36, 159.93, 153.65, 142.06, 140.85, 131.88, 131.83, 129.10, 129.02, 124.83, 124.76, 124.72, 124.67, 123.54, 115.66, 115.44, 32.32, 32.29; HRMS (ESI+) calculated for $C_{11}H_9BrFN_3$ $[M+H]^+$ m/z 282.0037, found 282.0033. HPLC 98.4% (AUC at 254 nm) 7.84 min (Synergi Max-RP, water/ACN 0.02%TFA).

***tert*-Butyl 2-((3-benzyl-5-bromopyrazin-2-yl)amino)-2-(diethoxyphosphoryl) acetate (compound 5a).** To a suspension of compound 4a (ref. [30]) (3.8 g, 14.4 mmol) in dichlorobenzene (30 ml), compound 2 (4.8 g, 17.3 mmol) and rhodium (II) acetate dimer (0.64 g, 1.44 mmol) were added. The mixture was heated to 105 °C for 72 h. After cooling, the mixture was diluted with ethyl acetate, concentrated with celite and purified with silica gel chromatography in heptane and ethyl acetate to afford the desired product (5.4 g, 73%) as a brown solid. ^{1}H NMR (400 MHz, $CDCl_3$) δ 8.05 (s, 1H), 7.38–7.21 (m, 5H), 5.27–5.19 (m, 1H), 5.01 (doublet of doublets (dd), J = 21.2, 8.0 Hz, 1H), 4.21–3.83 (m, 6H), 1.42 (s, 9H), 1.24 (doublet of triplets (dt), J = 21.2, 7.0 Hz, 6H); ^{13}C NMR (101 MHz, $CDCl_3$) δ 166.16, 150.27 (d, J = 8.5 Hz), 142.90, 141.66, 135.53, 129.01, 128.74, 127.18, 126.33, 83.11, 63.66–63.24 (m), 52.54 (d, J = 146 Hz), 40.38, 27.84, 16.35–16.27(m); HRMS (ESI+) calculated for $C_{21}H_{29}BrN_3O_5P$ $[M+H]^+$ m/z 514.1107, found 514.1085; HPLC 98.1% (AUC at 254 nm) 6.59 min (Synergi Max-RP, water/ACN 0.1%TFA).

***tert*-Butyl 2-((5-bromo-3-(2-fluorobenzyl)pyrazin-2-yl)amino)-2-(diethoxyphosphoryl)acetate (compound 5b).** To a suspension of compound 4b (1.3 g, 4.6 mmol) in dichlorobenzene (20 ml), compound 2 (1.9 g, 6.9 mmol) as well as rhodium (II) acetate dimer (0.20 g, 0.46 mmol) were added. The mixture was heated to 105 °C for 18 h. After cooling, the mixture was diluted with ethyl acetate, concentrated with celite and purified with silica gel chromatography in heptane and ethyl acetate to afford the desired product (2.2 g, 88%) as a brown solid. ^{1}H NMR (400 MHz, DMSO-d_6) δ 8.13 (s, 1H), 7.42–7.02 (m, 1H), 6.78 (dd, J = 8.6, 4.2 Hz, 1H), 5.10 (dd, J = 23.4, 8.6 Hz, 1H), 4.18 (s, 2H), 4.14–3.90 (m, 4H), 1.42 (s, 9H), 1.20 (dt, J = 28.2, 7.0 Hz, 6H); ^{13}C NMR (101 MHz, DMSO-d_6) δ 166.29, 162.25, 159.82, 150.93, 142.85, 141.27, 131.82, 129.35, 125.58, 124.92, 124.26, 115.79, 82.62, 63.44, 54.42, 52.96, 32.31, 27.98, 16.63; HRMS (ESI+) calculated for $C_{21}H_{28}BrFN_3O_5P$ $[M+H]^+$ m/z 532.1007, found 532.1001; HPLC 94.1% (AUC at 254 nm) 6.59 min (Synergi Max-RP, water/ACN 0.02%TFA).

***tert*-Butyl 2-((3-benzyl-5-bromopyrazin-2-yl)amino)-3-(furan-2-yl)acrylate (compound 6a).** To a solution of compound 5a (5.4 g, 10.5 mmol) in methanol (100 ml), furfural was added (1.5 g, 15.7 mmol). Tetramethylguanidine (3.6 g, 31.5 mmol) was added dropwise and the reaction stirred at room temperature for 30 min. The reaction was diluted with dichloromethane and poured into a separatory funnel with HCl (0.1 M). The two layers were separated and the aqueous layer was extracted with dichloromethane. The organic layers were combined, dried with sodium sulfate, filtered, concentrated and purified with silica gel chromatography in heptane and ethyl acetate to afford the desired product (4.0 g, 83%) as a brown solid. ^{1}H NMR (400 MHz, $CDCl_3$) δ 8.13 (s, 1H), 7.43–7.27 (m, 5H), 6.96 (d, J = 1.8 Hz, 1H), 6.90 (s, 1H), 6.70 (s, 1H), 6.29 (dd, J = 3.5, 1.8 Hz, 1H), 6.16 (d, J = 3.5 Hz, 1H), 4.27 (s, 2H), 1.45 (s, 9H); ^{13}C NMR (101 MHz, $CDCl_3$) δ 164.01, 150.36, 149.59, 143.83, 143.25, 142.11, 136.21, 129.23, 128.81, 128.33, 127.53, 127.31, 112.71, 111.70, 110.84, 81.70, 40.50, 27.91; HRMS (ESI+) calculated for $C_{22}H_{22}BrN_3O_3$ $[M+H]^+$ m/z 456.0924, found 456.0913; HPLC 94.1% (AUC at 254 nm) 6.86 min (Synergi Max-RP, water/ACN 0.1%TFA).

***tert*-Butyl 2-((5-bromo-3-(2-fluorobenzyl)pyrazin-2-yl)amino)-3-(furan-2-yl) acrylate (compound 6b).** To a solution of compound 5b (4.4 g, 8.3 mmol) in methanol (100 ml), furfural was added (0.95 g, 9.9 mmol). Tetramethylguanidine (2.9 g, 24.8 mmol) was added dropwise and the reaction stirred at room temperature for 30 min. The reaction was diluted with dichloromethane and poured into a separatory funnel with HCl (0.1 M). The two layers were separated and the aqueous layer was extracted with dichloromethane. The organic layers were combined, dried with sodium sulfate, filtered, concentrated and purified with silica gel chromatography in heptane and ethyl acetate to afford the desired product (2.8 g, 71%) as a light yellow gum. ^{1}H NMR (400 MHz, DMSO-d_6) δ 8.50 (s, 1H), 8.10 (s, 1H), 7.72 (d, J = 1.7 Hz, 1H), 7.42–7.13 (m, 4H), 7.04 (s, 1H), 6.79 (d, J = 3.5 Hz, 1H), 6.57 (t, J = 2.6 Hz, 1H), 4.24 (s, 2H), 1.34 (s, 9H); ^{13}C NMR (101 MHz, DMSO-d_6) δ 164.25, 162.31, 159.88, 150.93, 150.12, 144.93, 142.39, 141.69, 131.65, 129.25, 127.25, 126.03, 124.84, 117.59, 115.77, 115.56, 114.66, 112.86, 81.01, 27.97; HRMS (ESI+) calculated for $C_{22}H_{21}BrFN_3O_3$ $[M+H]^+$ m/z 474.0823, found 474.0812; HPLC 98.9% (AUC at 254 nm) 8.98 min (Synergi Max-RP, water/ACN 0.02%TFA).

***tert*-Butyl 2-((3-benzyl-5-(4-((*tert*-butyldimethylsilyl)oxy)phenyl)pyrazin-2-yl)amino)-3-(furan-2-yl)acrylate (compound 7a).** To a solution of compound 6a (0.24 g, 0.53 mmol) in dioxane (10 ml), (4-((*tert*-butyldimethylsilyl)oxy) phenyl)boronic acid (0.20 g, 0.79 mmol), (1,1′-bis(diphenylphosphino)ferrocen e)-dichloropalladium(II) (0.042 g, 0.053 mmol) and cesium carbonate (1.05 ml, 1.05 mmol, 1.0 M) were added. The mixture was purged with nitrogen and heated to 85 °C for 18 h. The reaction was diluted with ethyl acetate and water. The two layers were separated and the aqueous layer was extracted with ethyl acetate. The organic layers were combined, dried with sodium sulfate, filtered, concentrated and purified with silica gel chromatography in heptane and ethyl acetate to afford the desired product (0.085 g, 27%) as a yellow solid. ^{1}H NMR (400 MHz, $CDCl_3$) δ 8.44 (s, 1H), 7.92–7.84 (m, 2H), 7.43–7.30 (m, 5H), 7.04 (s, 1H), 7.00–6.93 (m, 3H), 6.71 (s, 1H), 6.67 (s, 1H), 6.29 (dd, J = 3.4, 1.8 Hz, 1H), 6.16 (d, J = 3.4 Hz, 1H), 4.40 (s, 2H), 1.45 (s, 9H), 1.03 (s, 9H), 0.25 (s, 6H); ^{13}C NMR (101 MHz, $CDCl_3$) δ 164.50, 156.40, 150.75, 148.56, 143.76, 142.91, 142.38, 137.15, 136.40, 130.19, 129.05, 128.88, 128.35, 127.34, 126.99, 120.54, 115.91, 112.08, 111.60, 109.61, 81.51, 40.86, 27.95, 25.76, 18.34; HRMS (ESI+) calculated for $C_{34}H_{41}N_3O_4Si$ $[M+H]^+$ m/z 584.2945, found 584.2941; HPLC 91.6% (AUC at 254 nm) 10.45 min (Zorbax XDB-C8, water/ACN 0.1%TFA).

***tert*-Butyl 2-((3-benzyl-5-(3-((*tert*-butyldimethylsilyl)oxy)phenyl)pyrazin-2-yl) amino)-3-(furan-2-yl)acrylate (compound 7b).** To a solution of compound 6a (0.32 g, 0.70 mmol) in dioxane (10 ml), (3-((*tert*-butyldimethylsilyl)oxy) phenyl)boronic acid (0.26 g, 1.05 mmol), (1,1′-bis(diphenylphosphino)ferroce ne)-dichloropalladium(II) (0.060 g, 0.070 mmol) and cesium carbonate (1.4 ml, 1.4 mmol, 1.0 M) were added. The mixture was purged with nitrogen and heated to 85 °C for 18 h. The reaction was diluted with ethyl acetate and water. The two layers were separated and the aqueous layer was extracted with ethyl acetate. The organic layers were combined, dried with sodium sulfate, filtered, concentrated and purified with silica gel chromatography in heptane and ethyl acetate to afford the desired product (0.265 g, 64%) as a dark brown foam. ^{1}H NMR (400 MHz, $CDCl_3$) δ 8.46 (s, 1H), 7.60–7.55 (m, 1H), 7.51–7.46 (m, 1H), 7.43–7.31 (m, 6H), 7.05 (s, 1H), 7.00 (d, J = 1.8 Hz, 1H), 6.89 (doublet of doublets of doublets (ddd), J = 8.1, 2.6, 1.0 Hz, 1H), 6.69 (s, 1H), 6.30 (dd, J = 3.4, 1.8 Hz, 1H), 6.17 (d, J = 3.4 Hz, 1H), 4.39 (s, 2H), 1.46 (s, 9H), 1.04 (s, 9H), 0.26 (s, 6H); ^{13}C NMR (101 MHz, $CDCl_3$) δ 164.48, 156.22, 150.70, 149.05, 143.46, 143.00, 142.50, 138.48, 137.11, 136.94, 129.90, 129.80, 129.06, 128.93, 128.17, 127.02, 120.07, 119.01, 117.76, 112.25, 111.64, 110.03, 81.57, 40.89, 27.91, 25.76, 18.29; HRMS (ESI+) calculated for $C_{34}H_{41}N_3O_4Si$ $[M+H]^+$ m/z 584.2945, found 584.2924; HPLC 88.5% (AUC at 254 nm) 10.43 min (Zorbax XDB-C8, water/ACN 0.1%TFA).

***tert*-Butyl 2-((3-benzyl-5-(3-nitrophenyl)pyrazin-2-yl)amino)-3-(furan-2-yl)acrylate (compound 7c).** To a solution of compound 6a (0.34 g, 0.75 mmol) in dioxane (10 ml), 3-nitrophenyl)boronic acid (0.19 g, 1.12 mmol), (1,1′-bis(diphenylphosphino)ferrocene)dichloropalladium(II) (0.061 g, 0.075 mmol) and cesium carbonate (1.5 ml, 1.5 mmol, 1.0 M) were added. The mixture was purged with nitrogen and heated to 85 °C for 1 h. The reaction was diluted with ethyl acetate and water. The two layers were separated and the aqueous layer was extracted with ethyl acetate. The organic layers were combined, dried with sodium sulfate, filtered, concentrated and purified with silica gel

chromatography in heptane and ethyl acetate to afford crude product (0.37 g) as an orange solid. ^{1}H NMR (400 MHz, $CDCl_3$) δ 8.88 (t, J = 2.0 Hz, 1H), 8.57 (s, 1H), 8.37–8.29 (m, 1H), 8.24 (ddd, J = 8.0, 2.0, 1.0 Hz, 1H), 7.65 (t, J = 8.0 Hz, 1H), 7.44–7.32 (m, 5H), 7.12 (s, 1H), 7.00 (d, J = 1.8 Hz, 1H), 6.73 (s, 1H), 6.31 (dd, J = 3.4, 1.8 Hz, 1H), 6.20 (d, J = 3.4 Hz, 1H), 4.41 (s, 2H), 1.42 (s, 9H); ^{13}C NMR (101 MHz, $CDCl_3$) δ 164.19, 150.44, 149.89, 148.95, 143.28, 142.92, 137.03, 136.63, 131.48, 130.31, 129.76, 129.18, 128.85, 127.60, 127.23, 123.32, 122.81, 120.76, 112.74, 111.73, 110.95, 81.71, 40.85, 27.97; HRMS (ESI+) calculated for $C_{28}H_{26}N_4O_5$ $[M+H]^+$ m/z 499.1982, found 499.1970. HPLC 70.9% (AUC at 254 nm) 6.45 min (Zorbax XDB-C8, water/ACN 0.1%TFA).

***tert*-Butyl 2-((3-benzyl-5-(3-((*tert*-butyldimethylsilyl)oxy)-2-fluorophenyl) pyrazin-2-yl)amino)-3-(furan-2-yl)acrylate (compound 7d).** To a solution of compound 6a (0.21 g, 0.46 mmol) in dioxane (10 ml), (3-((*tert*-butyldimethylsilyl) oxy)-2-fluorophenyl)boronic acid (0.19 g, 0.69 mmol), (1,1′-bis(diphenylphosphino) ferrocene)dichloropalladium(II) (0.037 g, 0.046 mmol) and cesium carbonate (0.92 ml, 0.92 mmol, 1.0 M) were added. The mixture was purged with nitrogen and heated to 85 °C for 3 h. The reaction was diluted with ethyl acetate and water. The two layers were separated and the aqueous layer was extracted with ethyl acetate. The organic layers were combined, dried with sodium sulfate, filtered, concentrated and purified with silica gel chromatography in heptane and ethyl acetate to desired product (0.16 g, 58%) as a white foam. ^{1}H NMR (400 MHz, DMSO-d_6) δ 8.46–8.21 (m, 2H), 7.63 (d, J = 1.6 Hz, 1H), 7.52–7.32 (m, 5H), 7.32–7.23 (m, 1H), 7.16 (t, J = 7.9 Hz, 1H), 7.08–6.91 (m, 2H), 6.60–6.39 (m, 2H), 4.34 (s, 2H), 1.32 (s, 9H), 0.98 (s, 9H), 0.21 (s, 6H); ^{13}C NMR (101 MHz, DMSO-d_6) δ 164.44, 152.91, 150.49, 150.22, 150.17, 144.62, 143.77, 143.64, 142.47, 140.04, 139.93, 138.44, 137.35, 129.37, 128.90, 127.73, 126.92, 126.43, 126.33, 124.97, 122.56, 121.88, 116.59, 114.15, 112.76, 80.86, 38.79, 27.90, 25.90, 18.49; HRMS (ESI+) calculated for $C_{34}H_{40}FN_3O_4Si$ $[M+H]^+$ m/z 602.2845, found 602.2827; HPLC 96.2% (AUC at 254 nm) 10.51 min (Synergi Max-RP, water/ACN 0.02%TFA).

***tert*-Butyl 2-((3-benzyl-5-(2-fluoro-3-nitrophenyl)pyrazin-2-yl)amino)-3-(furan-2-yl)acrylate (compound 7e).** To a solution of compound 6a (0.24 g, 0.53 mmol) in dioxane (10 ml), 2-(2-fluoro-3-nitrophenyl)-4,4,5,5-tetramethyl-1,3,2-dioxaborolane (0.21 g, 0.79 mmol), (1,1′-bis(diphenylphosphino)ferrocene) dichloropalladium(II) (0.042 g, 0.053 mmol) and cesium carbonate (1.6 ml, 1.6 mmol, 1.0 M) were added. The mixture was purged with nitrogen and heated to 85 °C for 1 h. The reaction was diluted with ethyl acetate and water. The two layers were separated and the aqueous layer was extracted with ethyl acetate. The organic layers were combined, dried with sodium sulfate, filtered, concentrated and purified with silica gel chromatography in heptane and ethyl acetate to desired product (0.19 g, 59%) as a yellow foam. ^{1}H NMR (400 MHz, DMSO-d_6) δ 8.53 (s, 1H), 8.42 (d, J = 2.7 Hz, 1H), 8.23 (td, J = 7.5, 6.6, 1.9 Hz, 1H), 8.14 (td, J = 7.7, 6.8, 1.8 Hz, 1H), 7.64 (d, J = 1.8 Hz, 1H), 7.54 (t, J = 8.0 Hz, 1H), 7.48–7.33 (m, 4H), 7.33–7.23 (m, 1H), 7.01 (s, 1H), 6.59–6.42 (m, 2H), 4.37 (s, 2H), 1.33 (s, 9H); ^{13}C NMR (101 MHz, DMSO-d_6) δ 164.34, 153.72, 151.10, 150.80, 150.10, 144.80, 142.80, 140.62, 138.69, 138.26, 135.98, 135.43, 129.38, 128.94, 127.95, 127.84, 127.39, 126.98, 125.93, 125.59, 117.29, 114.45, 112.80, 80.95, 38.70, 27.92; HRMS (ESI+) calculated for $C_{28}H_{25}FN_4O_5$ $[M+H]^+$ m/z 517.1882, found 517.1865; HPLC 98.5% (AUC at 254 nm) 9.78 min (Synergi Max-RP, water/ACN 0.02%TFA).

***tert*-Butyl 2-((5-(2-fluoro-3-nitrophenyl)-3-(2-fluorobenzyl)pyrazin-2-yl) amino)-3-(furan-2-yl)acrylate (compound 7f).** To a solution of compound 6b (2.6 g, 5.5 mmol) in dioxane (50 ml), 2-(2-fluoro-3-nitrophenyl)-4,4,5,5-tetramethyl-1,3,2-dioxaborolane (2.2 g, 8.2 mmol), (1,1′-bis(diphenylphosphino)ferrocene) dichloropalladium(II) (0.45 g, 0.55 mmol) and cesium carbonate (13.7 ml, 13.7 mmol, 1.0 M) were added. The mixture was purged with nitrogen and heated to 85 °C for 1 h. The reaction was diluted with ethyl acetate and water. The two layers were separated and the aqueous layer was extracted with ethyl acetate. The organic layers were combined, dried with sodium sulfate, filtered, concentrated and purified with silica gel chromatography in heptane and ethyl acetate to desired product (2.9 g, 97%) as a light brown solid. ^{1}H NMR (400 MHz, DMSO-d_6) δ 8.70 (s, 1H), 8.42 (d, J = 2.8 Hz, 1H), 8.17–7.92 (m, 2H), 7.73 (d, J = 1.7 Hz, 1H), 7.47 (t, J = 8.0 Hz, 1H), 7.41–7.13 (m, 4H), 7.06 (s, 1H), 6.82 (d, J = 3.5 Hz, 1H), 6.58 (dd, J = 3.5, 1.8 Hz, 1H), 4.36 (s, 2H), 1.35 (s, 9H); ^{13}C NMR (101 MHz, DMSO-d_6) δ 164.36, 162.46, 160.03, 153.67, 150.94, 150.19, 144.95, 141.36, 140.59, 138.68, 135.56, 135.23, 131.66, 129.05, 127.72, 127.38, 125.84, 125.50, 125.24, 124.76, 117.51, 115.66, 115.44, 114.66, 112.86, 80.98, 27.93; HRMS (ESI+) calculated for $C_{28}H_{24}F_2N_4O_5$ $[M+H]^+$ m/z 535.1788, found 535.1790; HPLC 90.9% (AUC at 254 nm) 9.11 min (Synergi Max-RP, water/ACN 0.02%TFA).

2-((3-Benzyl-5-(4-((*tert*-butyldimethylsilyl)oxy)phenyl)pyrazin-2-yl)amino)-3-(furan-2-yl)acrylic acid (compound 8a). To a solution of compound 7a (0.080 g, 0.14 mmol) in dichloromethane (10 ml), trifluoroacetic acid (1 ml) was added and the reaction stirred at room temperature for 6 h. The mixture was diluted with toluene and concentrated. The process was repeated twice to afford crude product as an orange oil. ESI MS m/z 528 $[M+H]^+$.

2-((3-Benzyl-5-(3-((*tert*-butyldimethylsilyl)oxy)phenyl)pyrazin-2-yl)amino)-3-(furan-2-yl)acrylic acid (compound 8b). To a solution of compound 7b (0.26 g, 0.45 mmol) in dichloromethane, (10 ml) trifluoroacetic acid (1 ml) was added and the reaction stirred at room temperature for 18 h. The mixture was diluted with toluene and concentrated. The process was repeated twice to afford crude product as an orange oil. ESI MS m/z 528 $[M+H]^+$.

2-((3-Benzyl-5-(3-nitrophenyl)pyrazin-2-yl)amino)-3-(furan-2-yl)acrylic acid (compound 8c). To a solution of compound 7c (0.26 g, 0.52 mmol) in dichloromethane, (10 ml) trifluoroacetic acid (1 ml) was added and the reaction stirred at room temperature for 1 h. The mixture was diluted with toluene and concentrated. The process was repeated twice to afford crude product as a brown solid. ESI MS m/z 443 $[M+H]^+$.

2-((3-Benzyl-5-(3-((*tert*-butyldimethylsilyl)oxy)-2-fluorophenyl)pyrazin-2-yl) amino)-3-(furan-2-yl)acrylic acid (compound 8d). To a solution of compound 7d (0.16 g, 0.26 mmol) in dichloromethane (10 ml), trifluoroacetic acid (1 ml) was added and the reaction stirred at room temperature for 2 h. The mixture was diluted with toluene and concentrated. The process was repeated twice to afford crude product as a brown solid. ESI MS m/z 546 $[M+H]^+$.

2-((3-Benzyl-5-(2-fluoro-3-nitrophenyl)pyrazin-2-yl)amino)-3-(furan-2-yl) acrylic acid (compound 8e). To a solution of compound 7e (1.7 g, 3.3 mmol) in dichloromethane (50 ml), trifluoroacetic acid (5 ml) was added and the reaction stirred at room temperature for 5 h. The mixture was diluted with toluene and concentrated. The process was repeated twice to afford crude product as a brown solid. ESI MS m/z 461 $[M+H]^+$.

2-((5-(2-Fluoro-3-nitrophenyl)-3-(2-fluorobenzyl)pyrazin-2-yl)amino)-3-(furan-2-yl)acrylic acid (compound 8f). To a solution of compound 7f (0.67 g, 1.3 mmol) in dichloromethane (20 ml), trifluoroacetic acid (2 ml) was added and the reaction stirred at room temperature for 3 h. The mixture was diluted with toluene and concentrated. The process was repeated twice to afford crude product as a brown foam. ESI MS m/z 479 $[M+H]^+$.

8-Benzyl-6-(4-((*tert*-butyldimethylsilyl)oxy)phenyl)-2-(furan-2-ylmethylene) imidazo(1,2-a)pyrazin-3(2H)-one (compound 9a). To a solution of compound 8a (0.14 mmol) in dichloromethane (10 ml), carbonyldiimidazole (44 mg, 0.27 mmol) was added and the reaction stirred at room temperature for 10 min. The reaction was diluted with dichloromethane and poured into a separatory funnel with HCl (0.1 M). The two layers were separated and the aqueous layer was extracted with dichloromethane. The organic layers were combined, dried with sodium sulfate, filtered and concentrated to afford crude product as a black solid. ESI MS m/z 510 $[M+H]^+$.

8-Benzyl-6-(3-((*tert*-butyldimethylsilyl)oxy)phenyl)-2-(furan-2-ylmethylene) imidazo(1,2-a)pyrazin-3(2H)-one (compound 9b). To a solution of compound 8b (0.45 mmol) in dichloromethane (10 ml), carbonyldiimidazole (147 mg, 0.91 mmol) was added and the reaction stirred at room temperature for 1 h. The reaction was diluted with dichloromethane and poured into a separatory funnel with HCl (0.1 M). The two layers were separated and the aqueous layer was extracted with dichloromethane. The organic layers were combined, dried with sodium sulfate, filtered and concentrated to afford crude product as a black solid. ESI MS m/z 510 $[M+H]^+$.

8-Benzyl-2-(furan-2-ylmethylene)-6-(3-nitrophenyl)imidazo(1,2-a)pyrazin-3(2H)-one (compound 9c). To a solution of compound 8c (0.52 mmol) in dichloromethane (10 ml), carbonyldiimidazole (168 mg, 1.04 mmol) was added and the reaction stirred at room temperature for 30 min. The reaction was diluted with dichloromethane and poured into a separatory funnel with HCl (0.1 M). The two layers were separated and the aqueous layer was extracted with dichloromethane. The organic layers were combined, dried with sodium sulfate, filtered and concentrated to afford crude product as a red black solid. ESI MS m/z 425 $[M+H]^+$.

8-Benzyl-6-(3-((*tert*-butyldimethylsilyl)oxy)-2-fluorophenyl)-2-(furan-2-ylmethylene)imidazo(1,2-a)pyrazin-3(2H)-one (compound 9d). To a solution of compound 8d (0.26 mmol) in dichloromethane (10 ml), carbonyldiimidazole (84 mg, 0.52 mmol) was added and the reaction stirred at room temperature for 1 h. The reaction was diluted with dichloromethane and poured into a separatory funnel with HCl (0.1 M). The two layers were separated and the aqueous layer was extracted with dichloromethane. The organic layers were combined, dried with sodium sulfate, filtered and concentrated to afford crude product as a red brown solid. ESI MS m/z 528 $[M+H]^+$.

8-Benzyl-6-(2-fluoro-3-nitrophenyl)-2-(furan-2-ylmethylene)imidazo(1,2-a) pyrazin-3(2H)-one (compound 9e). To a solution of compound 8e (3.3 mmol) in dichloromethane (100 ml), carbonyldiimidazole (1.1 g, 6.7 mmol) was added and the reaction stirred at room temperature for 2 h. The reaction was diluted with dichloromethane and poured into a separatory funnel with HCl (0.1 M). The two layers were separated and the aqueous layer was extracted with dichloromethane.

The organic layers were combined, dried with sodium sulfate, filtered and concentrated to afford crude product as a red brown solid. ESI MS *m/z* 443 $[M+H]^+$.

6-(2-Fluoro-3-nitrophenyl)-8-(2-fluorobenzyl)-2-(furan-2-ylmethylene) imidazo(1,2-a)pyrazin-3(2H)-one (compound 9f). To a solution of compound 8f (1.3 mmol) in dichloromethane (20 ml), carbonyldiimidazole (0.41 g, 2.5 mmol) was added and the reaction stirred at room temperature for 30 min. The reaction was diluted with dichloromethane and poured into a separatory funnel with HCl (0.1 M). The two layers were separated and the aqueous layer was extracted with dichloromethane. The organic layers were combined, dried with sodium sulfate, filtered and concentrated to afford crude product as a red brown solid. ESI MS *m/z* 461 $[M+H]^+$.

8-Benzyl-6-(4-((*tert*-butyldimethylsilyl)oxy)phenyl)-2-(furan-2-ylmethyl) imidazo(1,2-a)pyrazin-3(7H)-one (compound 10a). To a solution of compound 9a (0.14 mmol) in dichloromethane/methanol (1:1, 10 ml) at 0 °C, sodium borohydride (26 mg, 0.69 mmol) was added and the reaction stirred for 10 min. The reaction was diluted with dichloromethane and poured into a separatory funnel with HCl (0.1 M). The two layers were separated and the aqueous layer was extracted with dichloromethane. The organic layers were combined, dried with sodium sulfate, filtered and concentrated to afford crude product as an orange solid. ESI MS *m/z* 512 $[M+H]^+$.

8-Benzyl-6-(3-((*tert*-butyldimethylsilyl)oxy)phenyl)-2-(furan-2-ylmethyl) imidazo(1,2-a)pyrazin-3(7H)-one (compound 10b). To a solution of compound 9b (0.45 mmol) in dichloromethane/methanol (1:1, 20 ml) at 0 °C, sodium borohydride (85 mg, 2.3 mmol) was added and the reaction stirred for 45 min. The reaction was diluted with dichloromethane and poured into a separatory funnel with HCl (0.1 M). The two layers were separated and the aqueous layer was extracted with dichloromethane. The organic layers were combined, dried with sodium sulfate, filtered and concentrated to afford crude product as a red brown solid. ESI MS *m/z* 512 $[M+H]^+$.

8-Benzyl-2-(furan-2-ylmethyl)-6-(3-nitrophenyl)imidazo(1,2-a)pyrazin-3(7H)-one (compound 10c). To a solution of compound 9c (0.52 mmol) in dichloromethane/methanol (1:1, 20 ml) at 0 °C, sodium borohydride (98 mg, 2.6 mmol) was added and the reaction stirred for 30 min. The reaction was diluted with dichloromethane and poured into a separatory funnel with HCl (0.1 M). The two layers were separated and the aqueous layer was extracted with dichloromethane. The organic layers were combined, dried with sodium sulfate, filtered and concentrated to afford crude product as a red brown solid. ESI MS *m/z* 427 $[M+H]^+$.

8-Benzyl-6-(3-((*tert*-butyldimethylsilyl)oxy)-2-fluorophenyl)-2-(furan-2-ylmethyl)imidazo(1,2-a)pyrazin-3(7H)-one (compound 10d). To a solution of compound 9d (0.26 mmol) in dichloromethane/methanol (1:1, 20 ml) at 0 °C, sodium borohydride (49 mg, 1.3 mmol) was added and the reaction stirred for 15 min. The reaction was diluted with dichloromethane and poured into a separatory funnel with HCl (0.1 M). The two layers were separated and the aqueous layer was extracted with dichloromethane. The organic layers were combined, dried with sodium sulfate, filtered and concentrated to afford crude product as a red brown solid. ESI MS *m/z* 530 $[M+H]^+$.

8-Benzyl-6-(2-fluoro-3-nitrophenyl)-2-(furan-2-ylmethyl)imidazo(1,2-a) pyrazin-3(7H)-one (compound 10e). To a solution of compound 9e (3.3 mmol) in dichloromethane/methanol (1:1, 20 ml) at 0 °C, sodium borohydride (0.64 mg, 16.7 mmol) was added and the reaction stirred for 30 min. The reaction was diluted with dichloromethane and poured into a separatory funnel with HCl (0.1 M). The two layers were separated and the aqueous layer was extracted with dichloromethane. The organic layers were combined, dried with sodium sulfate, filtered and concentrated to afford crude product as a red brown solid. ESI MS *m/z* 445 $[M+H]^+$.

6-(2-Fluoro-3-nitrophenyl)-8-(2-fluorobenzyl)-2-(furan-2-ylmethyl) imidazo(1,2-a)pyrazin-3(7H)-one (compound 10f). To a solution of compound 9f (1.3 mmol) in dichloromethane/methanol (1:1, 20 ml) at 0 °C, sodium borohydride (0.12 mg, 3.1 mmol) was added and the reaction stirred for 30 min. The reaction was diluted with dichloromethane and poured into a separatory funnel with HCl (0.1 M). The two layers were separated and the aqueous layer was extracted with dichloromethane. The organic layers were combined, dried with sodium sulfate, filtered and concentrated to afford crude product as a red brown solid. ESI MS *m/z* 463 $[M+H]^+$.

8-Benzyl-2-(furan-2-ylmethyl)-6-(4-hydroxyphenyl)imidazo(1,2-a)pyrazin-3(7H)-one (compound A). To a solution of compound 10a (0.14 mmol) in methanol (10 ml), HCl (1 ml, 6 M) was added and the reaction stirred at room temperature for 1 h. The reaction was diluted with dichloromethane and poured into a separatory funnel with water. The two layers were separated and the aqueous layer was extracted with dichloromethane. The organic layers were combined, dried with sodium sulfate, filtered, concentrated and purified with silica gel chromatography in dichloromethane and methanol to afford the desired product (0.040 g, 74% over four steps) as an orange solid. ^{1}H NMR (400 MHz, CD_3OD) δ 7.84 (s, 1H), 7.60–7.51 (m, 2H), 7.46–7.38 (m, 3H), 7.37–7.29 (m, 2H), 7.29–7.20 (m, 1H), 6.95–6.87 (m, 2H), 6.34 (dd, J = 3.2, 1.9 Hz, 1H), 6.14 (d, J = 3.2 Hz, 1H), 4.48 (s, 2H), 4.24 (s, 2H); HRMS (ESI+) calculated for $C_{24}H_{19}N_3O_3$ $[M+H]^+$ *m/z* 398.1505, found 398.1498; HPLC 97.1% (AUC at 254 nm) 4.45 min (Synergi Max-RP, water/ACN 0.1%TFA).

8-Benzyl-2-(furan-2-ylmethyl)-6-(3-hydroxyphenyl)imidazo(1,2-a)pyrazin-3(7H)-one (compound B, hydrofurimazine). To a solution of compound 10b (0.45 mmol) in methanol (20 ml), HCl (1 ml, 6 M) was added and the reaction stirred at room temperature for 1 h. The reaction was diluted with dichloromethane and poured into a separatory funnel with water. The two layers were separated and the aqueous layer was extracted with dichloromethane. The organic layers were combined, dried with sodium sulfate, filtered, concentrated and purified with silica gel chromatography in dichloromethane and methanol to afford the desired product (0.091 g, 50% over four steps) as a brown solid. ^{1}H NMR (400 MHz, CD_3OD) δ 7.71 (s, 1H), 7.47–7.38 (m, 3H), 7.37–7.21 (m, 4H), 7.18–7.04 (m, 2H), 6.90 (ddd, J = 8.1, 2.4, 0.9 Hz, 1H), 6.34 (dd, J = 3.2, 1.9 Hz, 1H), 6.18–6.09 (m, 1H), 4.44 (s, 2H), 4.21 (s, 2H); ^{13}C NMR (400 MHz, CD_3OD); δ 157.79, 149.70, 147.30, 142.15, 139.11, 138.69, 135.47, 134.51, 129.77, 128.96, 128.44, 126.99, 126.79, 121.74, 117.55, 116.58, 113.35, 110.33, 110.29, 107.02, 37.17, 23.14; HRMS (ESI+) calculated for $C_{24}H_{19}N_3O_3$ $[M+H]^+$ *m/z* 398.1505, found 398.1503; HPLC 97.1% (AUC at 254 nm) 4.55 min (Synergi Max-RP, water/ACN 0.1%TFA).

6-(3-Aminophenyl)-8-benzyl-2-(furan-2-ylmethyl)imidazo(1,2-a)pyrazin-3(7H)-one (compound C). To a nitrogen purged solution of compound 10c (1.0 mmol) in methanol (50 ml), Pd/C (40 mg) was added. The mixture was purged with hydrogen and then stirred with 1 atm hydrogen for 4 h at room temperature. The mixture was purged with nitrogen, filtered over celite, concentrated and purified with silica gel chromatography in dichloromethane and methanol to afford the desired product (0.24 g, 59% over four steps) as a dark orange solid. ^{1}H NMR (400 MHz, CD_3OD) δ 7.64 (s, 1H), 7.47–7.37 (m, 3H), 7.36–7.28 (m, 2H), 7.28–7.14 (m, 2H), 6.94 (s, 1H), 6.89 (d, J = 7.6 Hz, 1H), 6.78 (ddd, J = 8.1, 2.4, 0.9 Hz, 1H), 6.33 (dd, J = 3.2, 1.9 Hz, 1H), 6.13 (dd, J = 3.2, 1.0 Hz, 1H), 4.43 (s, 2H), 4.21 (s, 2H); HRMS (ESI+) calculated for $C_{24}H_{20}N_4O_2$ $[M+H]^+$ *m/z* 397.1665 found 397.1659; HPLC 94.1% (AUC at 254 nm) 3.87 min (Synergi Max-RP, water/ACN 0.1%TFA).

8-Benzyl-6-(2-fluoro-3-hydroxyphenyl)-2-(furan-2-ylmethyl)imidazo(1,2-a) pyrazin-3(7H)-one (compound D). To a solution of compound 10d (0.26 mmol) in methanol (20 ml), HCl (1 ml, 6 M) was added and the reaction stirred at room temperature for 2 h. The reaction was diluted with dichloromethane and poured into a separatory funnel with water. The two layers were separated and the aqueous layer was extracted with dichloromethane. The organic layers were combined, dried with sodium sulfate, filtered, concentrated and purified with silica gel chromatography in dichloromethane and methanol to afford the desired product (0.071 g, 66% over four steps) as an orange brown solid. ^{1}H NMR (400 MHz, Methanol-d_4) δ 7.72 (s, 1H), 7.50–7.37 (m, 3H), 7.37–7.19 (m, 3H), 7.19–6.98 (m, 3H), 6.34 (dd, J = 3.2, 1.9 Hz, 1H), 6.13 (dd, J = 3.2, 1.0 Hz, 1H), 4.42 (s, 2H), 4.22 (d, J = 1.0 Hz, 2H); HRMS (ESI+) calculated for $C_{24}H_{18}FN_3O_3$ $[M+H]^+$ *m/z* 416.1405, found 416.1384; HPLC 99.6% (AUC at 254 nm) 4.45 min (Synergi Max-RP, water/ACN 0.1%TFA).

6-(3-Amino-2-fluorophenyl)-8-benzyl-2-(furan-2-ylmethyl)imidazo(1,2-a) pyrazin-3(7H)-one (compound E). To a nitrogen purged solution of compound 10e (3.3 mmol) in methanol (50 ml), Pd/C (40 mg) was added. The mixture was purged with hydrogen and then stirred with 1 atm hydrogen for 4 h at room temperature. The mixture was purged with nitrogen, filtered over celite, concentrated and purified with silica gel chromatography in dichloromethane and methanol to afford the desired product (0.17 g, 12% over four steps) as a dark orange solid. ^{1}H NMR (400 MHz, methanol-d_4) δ 7.67 (s, 1H), 7.48–7.37 (m, 3H), 7.37–7.20 (m, 3H), 7.10–6.90 (m, 2H), 6.83 (s, 1H), 6.34 (dd, J = 3.2, 1.9 Hz, 1H), 6.13 (dd, J = 3.3, 1.0 Hz, 1H), 4.41 (s, 2H), 4.22 (d, J = 0.9 Hz, 2H); HRMS (ESI+) calculated for $C_{24}H_{19}FN_4O_2$ $[M+H]^+$ *m/z* 415.1565 found 415.1546; HPLC 100% (AUC at 254 nm) 4.47 min (Synergi Max-RP, water/ACN 0.1%TFA).

6-(3-Amino-2-fluorophenyl)-8-(2-fluorobenzyl)-2-(furan-2-ylmethyl) imidazo(1,2-a)pyrazin-3(7H)-one (compound F, fluorofurimazine). To a nitrogen purged solution of compound 10f (1.3 mmol) in methanol (20 ml), Pd/C (40 mg) was added. The mixture was purged with hydrogen and then stirred with 1 atm hydrogen for 6 h at room temperature. The mixture was purged with nitrogen, filtered over celite, concentrated and purified with silica gel chromatography in dichloromethane and methanol to afford the desired product (0.28 g, 51% over four steps) as an orange brown solid. ^{1}H NMR (400 MHz, methanol-d_4) δ 7.81 (s, 1H), 7.39 (d, J = 1.8 Hz, 1H), 7.36–7.25 (m, 2H), 7.18–7.07 (m, 2H), 7.06–6.80 (m, 3H), 6.33 (dd, J = 3.2, 1.9 Hz, 1H), 6.11 (dd, J = 3.0, 1.0 Hz, 1H), 4.49 (s, 2H), 4.20 (s, 2H); ^{13}C NMR (101 MHz, CD_3OD) δ 162.50, 160.06,

154.96, 152.43, 149.24, 147.42, 142.35, 137.77, 135.20, 135.18, 131.70, 131.66, 130.99, 130.97, 129.24, 129.16, 126.51, 125.96, 125.45, 125.41, 124.19, 124.17, 124.15, 124.08, 122.57, 122.41, 119.71, 119.57, 116.55, 114.94, 114.73, 114.18, 114.04, 110.39, 107.21, 32.09, 22.26; HRMS (ESI+) calculated for $C_{24}H_{18}F_2N_4O_2$ $[M+H]^+$ *m/z* 433.1471 found 433.1454; HPLC 95.0% (AUC at 254 nm) 6.57 min (Luna C8, water/ACN 0.1%TFA).

Spectral analysis of Antares and furimazine analogs. A single colony of Antares plasmid in KRX *E. coli* cells was used to inoculate a liquid culture in LB broth, which was grown for 18 h at 37 °C. The culture was then diluted 1:100 into a flask containing 500 ml of Terrific Broth and grown for an additional 4 h at 37 °C. Protein expression was induced by the addition of 0.1% rhamnose with growth for 65 h at 15 °C. Cells were pelleted and resuspended in a buffer containing Tris-buffered saline with 0.2 mg ml^{-1} lysozyme. Cells were lysed by three freeze-thaw cycles. After the final thaw, 0.001 U ml^{-1} RNAse-free DNase (RQ1, Promega) was added and the sample was incubated on ice for 30 min. The lysate was centrifuged, and the cleared supernatant was loaded to a 1-ml nickel-Sepharose column and then washed with 6 column volumes of buffer. Next, 1-ml fractions were collected and pooled. The pooled fractions were loaded onto a 5-ml Phenyl Sepharose (High Sub) column (GE Healthcare) for hydrophobic interaction chromatography. Fractions were orange coloration were collected and the pooled fractions were loaded to a 1-ml HiTrap Q column (GE Healthcare) for anion exchange chromatography. Fractions with orange coloration were collected and the pooled material was quantitated and stored at −20 °C.

To measure emission spectra with furimazine and new substrates, the purified Antares protein was diluted to 100 pM in Dulbecco's phosphate-buffered saline (DPBS) (Life Technologies 14190) with 0.01% fetal bovine serum (FBS) (Life Technologies). Each substrate was diluted to 25 µmol into DPBS with 0.01% FBS. Then 50 µl of the Antares dilution was combined with 50 µl of each substrate in triplicate. Finally, the spectral profile from 400 to 700 nm was acquired using an Infinite M-1000 luminometer (TECAN).

Enzymatic analysis of Antares and furimazine analogs. A single colony of Antares plasmid in KRX *E. coli* was grown for 18 h at 37 °C in LB broth. The overnight culture was diluted 1:100 into a flask containing 50 ml of Terrific Broth and grown for 4 h at 37 °C. Protein expression was induced by the addition of 0.1% Rhamnose with growth for 24 h at 15 °C. Cells were collected by centrifugation and then resuspended in 9 ml of 100 mM HEPES pH 7.5 with 0.001 U ml^{-1} RQ1 DNase (Promega M6101). Cells were lysed by the addition of 1 ml of 10× FastBreak Cell Lysis Reagent (Promega V8571) and then placed on a rotating mixer for 1 h at 4 °C. A cleared lysate was prepared by centrifugation at 7,000 r.p.m. for 15 min. The cleared lysate was then purified using further using the MagneHis Protein Purification System (Promega V8500) according to the manufacturer's protocols.

To quantify luminescence as a function of substrate concentration, purified Antares protein was diluted to 100 pM in DPBS with 0.01% FBS. Substrates were diluted to 25 µmol and then serially diluted in twofold steps into DPBS with 0.01% FBS in triplicate. The 50 µl of diluted Antares protein was then combined with 50 µl of each substrate dilution. Luminescence was measured immediately using a GloMax-Multi+ luminometer (Promega). Kinetic parameters of K_M and V_{max} were calculated using the Michaelis–Menten nonlinear regression function in the program Prism (GraphPad).

To monitor signal decay over time, purified Antares protein was diluted to 100 pM in DPBS with 0.01% FBS. Each substrate was diluted to 25 µmol into DPBS with 0.01% FBS in triplicate. Next, 50 µl of the Antares dilution was combined with 50 µl each substrate dilution. Luminescence was measured immediately using the GloMax-Multi+ luminometer and then samples were measured every 2 min for 60 min to monitor signal decay over time.

Substrate stability. Each substrate was diluted to 25 µmol in either DPBS or DPBS with 10% FBS. Aliquots of the diluted substrates were made in wells of a thin walled 96-well PCR tray, which was then placed in a thermocycler set to incubate at 37 °C. At various times, 10 µl of each sample was added to 90 µl of a diluted NanoLuc solution in triplicate. When the luminescence measurements were complete, the half-life of each substrate was calculated by fitting to a one-phase decay function in the program Prism with asymptope set to zero.

Solubility testing. To compare the solubility of Fz analogs in the injectable formulation of 10% ethanol (v/v), 10% glycerol(v/v), 10% 2-Hydroxypropyl-β-cyclodextrin (HPBCD, w/v), 35% PEG-300 (v/v) in water, preweighed compound was dissolved or suspended in ethanol and then combined with a mixture of the other components, followed by 15 min of agitation on a vortex mixer, to create a 28 mM solution or suspension. Suspensions with undissolved solids were heated to 50 °C for 15 min to promote solubilization. More dilute solutions or suspensions were created by dilution into premixed injectable formulation.

Solid formulation for use in whole-animal imaging. Stock samples of solid formulated HFz and FFz were prepared as follows. First, 120 mg of poloxamer-407 (Pluronic F127) were placed into a glass, screw-cap vial. The polymer was then heated to 80 °C in a water bath until melted. HFz or FFz (18 mg) dissolved in 400 µl of ethanol was added to the hot polymer, mixing well with a thin spatula. Additional rinses of HFz or FFz in ethanol was added to the hot polymer for quantitative transfer. The solvent was then removed under vacuum. This concentrated sample was diluted with 4.5 ml of water to make a master stock of ~9 mM HFz or FFz in water. Next, 480 µl of this aqueous stock was then aliquoted into glass vials, frozen and lyophilized overnight to give a yellow cake. For an i.p. injection into mice, 480 µl water was added to the vial and vortexed to create a clear solution, giving a single dose of 12 mg poloxamer-407 and 4.3 µmol HFz, or three doses of 4 mg poloxamer-407 and 1.3 µmol FFz.

Generation of luciferase-expressing stable tumor cell lines. HeLa cells were cultured at 37 °C with 5% CO_2 in Dulbecco's Modified Eagle's Medium (DMEM) supplemented with 10% FBS, 2 mM L-glutamate, 100 U ml^{-1} penicillin and 100 µg ml^{-1} streptomycin. EW8 or MG63.3 cell lines were cultured at 37 °C with 5% CO_2 in RPMI 1640 (RPMI) supplemented with 2 mM L-glutamate and 25 mM HEPES (Gibco) and 10% FBS, 100 U ml^{-1} penicillin, 100 µg ml^{-1} streptomycin and 5 µg ml^{-1} plasmocin. HeLa cells and EW8 cells were lentiviral transfected with pLL3.7m-CMV-Antares-P2A-AkaLuc-WPRE, pLL3.7m-CMV-Antares-P2A-Blasticidin or pLL3.7m-CMV-AkaLuc-P2A-Blasticidin, MG63.3 cells were retroviral transfected with pMSCV-AkaLuc-mNeonGreen or pMSCV-Antares-mNeonGreen. Then, 72 h after transfection, cells were dissociated with trypsin and resuspended in DMEM and then changed to PBS. Suspended cells were sorted for the top 5% brightest population on a fluorescence-activated cell sorter (FACS), the FACSJazz (BD Biosciences). Stable polyclonal cell lines were generated after ~1–2 weeks with 1–3 rounds of cell sorting. Flow cytometry data were analyzed on FlowJo software.

Retroviral vector production and T cell transduction. To generate retroviral supernatants, 293GP cells were transiently transfected with the CAR plasmid and the RD114 envelope plasmid, as previously described[31]. T cells were isolated from healthy human buffy coats by negative selection using the RosetteSep Human T Cell Enrichment Cocktail kit (STEMCELL Technologies). The T cells were activated with Dynabeads Human T-Expander CD3/CD28 (ThermoFisher Scientific) and cultured in T cell media (AIM V (ThermoFisher Scientific) +5% FBS (Sigma-Aldrich), 100 U ml^{-1} rhIL-2 (PeproTech), 2 mM L-glutamine, 100 U ml^{-1} penicillin, 10 mg ml^{-1} streptomycin and 10 mM HEPES). T cells were cultured on virus-coated Retronectin plates (Takara) on days 2 and 3 after activation to introduce the CAR transgene. Beads were magnetically removed on day 4 and the T cells were expanded in T cell media until day 7.

In vitro cell-based bioluminescence characterization. Luciferase-expressing stable tumor cells were seeded into 96-well Lumitrac plate (Greiner Bio-One) at a density of 8×10^4 cells per well. After 24 h, cells were washed with PBS and changed to 50 µl OptiMEM. For assaying NanoLuc-based reporter luminescence, Nano-Glo Live cell assay system (Promega) was used following the manufacturer's instructions. For assaying AkaLuc reporter luminescence, a final concentration of 150 µmol AkaLumine was added to each well. Time-lapse live-cell luminescence was recorded on an Infinite M-1000 luminometer (TECAN) with 100 ms integration and one read per min for 20 min.

Generation of reporter mice. The Antares coding sequence was amplified by PCR from a pBAD-His-Antares template in which the last 12 codons (encoding NLGGGMDELYK) were sequence-diversified to allow unique priming, using forward primer 5′-TCTTCACAGGCCAACGCGTATGGTGAGCAA GGGCGAGGAGCTGATCAA-3′ and reverse primer 5′-TTATCTAGAATTCTC GCGATTACTTATAGAGTTCATCCATTCCGCCACCGAGATT-3′ (start and stop codons underlined). Primers were designed for a recombineering reaction with pBT378-LSL+ plasmid digested with MluI and NruI, and so contained 5′ sequences matching pBT378-LSL+ immediately outside MluI and NruI sites. The PCR product and digested pBT378-LSL+ plasmid were purified by agarose gel electrophoresis and elution, the fragments recombined using In-Fusion reagent (Takara Clontech) to create pBT378-LSL-Antares and the reaction was transformed into XL-10 Gold *E. coli* competent cells (Agilent). Plasmids purified from individual cultures were checked by the presence of the insert by digestion by MluI and NruI, and then sequenced through the Antares open reading frame to ensure no mutations were introduced. To create pBT378-LSL-FLuc, a FLuc-coding sequence (*Luc2* mammalian expression-optimized codon variant) was amplified by PCR with forward primer 5′-TTCACAGGCCAACGCGTGCCACCATG GAAGATGCCAAAAACATTAAGAAG-3′ and reverse primer 5′-ATCTAGAATTCTCGCGATTACACGGCGATCTTGCCGCCCTTCTT-3′, and recombined with pBT378-LSL$^+$ digested with MluI and NruI as before. In pBT378-LSL-Antares or pBT378-LSL-FLuc, the reporter coding sequence is placed downstream of the CAG enhancer-promoter-intron and a loxP-stop-loxP (LSL) cassette, and upstream of a SV40 polyadenylation signal. This entire transcriptional unit is flanked by attB sites for integration by φC31 integrase into attP sites.

The plasmids pBT378-LSL-Antares and pBT378-LSL-FLuc were then used by the Stanford Transgenic, Knockout and Tumor Model Center for injection together with φC31 integrase mRNA into pronuclear zygotes of C57BL/6J mice

homozygous for three copies of the attP site at the *H11* locus (*H11P*) as previously described[17]. For both Antares and FLuc, two mice derived from different injected zygotes were verified to contain the desired inserts at *H11P* by PCR. These transgenes were designated *H11P-CAG-LSL-Antares-A*, *H11P-CAG-LSL-Antares-B*, *H11P-CAG-LSL-FLuc-A* and *H11P-CAG-LSL-FLuc-B*. Each founder was crossed to wild-type C57BL/6J mice, and transgene-positive male and female progeny were mated to each other to obtain homozygous lines. For reporter expression in kidney or liver, homozygous reporter line were crossed to *nestin-Cre* transgenic mice (mixture of C57Bl/6J and CD1 strains, gift of Liqun Luo, Stanford University) or *albumin-Cre* transgenic mice (FVB-N strain, gift of Karl Sylvester, Stanford University), respectively. The progeny, which were hemizygous for both driver and reporter genes, were then used for bioluminescence imaging experiments. Mice bearing *H11P-CAG-LSL-Antares-A* and *-B* transgenes produced similar imaging results in pilot experiments, and both were used for the experiments reported in this study. Likewise, mice bearing *H11P-CAG-LSL-FLuc-A* and *-B* transgenes produced similar imaging results in pilot experiments, but *H11P-CAG-LSL-FLuc-B* homoygotes produced larger litters and so only mice bearing the *H11P-CAG-LSL-FLuc-B* transgene were used for the experiments reported in this study.

Bioluminescence imaging of transgenic mice for substrate comparison. For substrate comparisons, transgenic mice doubly hemizygous for *albumin-Cre* or *nestin-Cre* and *CAG-LSL-Antares* or *CAG-LSL-FLuc*, wild-type C57BL/6J mice, nestin-cre mice or hemizygous DAT-cre mice (mixture of B6 and C57Bl/6J, a gift from J. Ding, Stanford University) of 2–4 months of age were anesthetized by inhalation of isoflurane for 5 min. An electric shaver was used to remove abdominal hair in *albumin-Cre* mice or dorsal hair in *nestin-Cre* mice. Nair depilatory cream (Church and Dwight) was then applied to the shaved area for 1 min, and remaining hair was removed with a piece of sterile gauze. The area was then rinsed with DPBS and cleaned with 70% ethanol with a piece of sterile gauze. For mice expressing Antares or negative control mice, indicated amounts of furimazine or furimazine analogs were dissolved in 480 µl of a polyethylene glycol-300 (PEG-300)-based formulation consisting of 10% glycerol, 10% ethanol, 10% hydroxypropylcyclodextrin and 35% PEG-300 in water. For mice expressing FLuc or negative control mice, indicated amounts of D-luciferin were dissolved in 414 µl of PBS. Substrates were then injected into the peritoneal cavity in the left lower quadrant. Immediately after substrate injection, bioluminescent images were acquired in an Ami HT bioluminescence imaging system (Spectral Instruments Imaging) for 15–30 min at intervals of 1 min. Imager settings were: (Low sensitivity settings) Emission filter, open; field of view, 25 cm; f-stop 8; binning, 1×1; and exposure time, 1 s. (High sensitivity settings) Emission filter, open; field of view, 25 cm; f-stop 1.2; binning, 2×2 and exposure time, 60 s. Images were analyzed in the Fiji version of the ImageJ program (NIH)[32], with further analysis in the program Excel (Microsoft). For each substrate, the average brightness with standard error of the mean (s.e.m.) error bars was plotted over time.

Hydrodynamic transfection and bioluminescence imaging of nude mice. To generate mammalian expression plasmids encoding luciferases, Antares coding sequence was PCR amplified as stated above, AkaLuc coding sequence was PCR amplified from a codon-optimized synthetic gblock (Integrated DNA Technology), LumiScarlet and Antares2 were PCR amplified from previously published plasmids (Addgene no. 126623, no. 100027). All luciferase coding sequences has a Kozak sequence appended before the start codon during PCR amplification. The resulted agarose gel purified DNA fragments were recombined with a backbone-modified pcDNA3.1 (Addgene no. 124095) vector linearized by KpnI and EcoRI, using In-Fusion reagent (Takara Clontech) to create pcDNA3.1-CAG-Antares/AkaLuc/LumiScarlet/Antares2.

For luciferase comparisons, livers of male 7-week-old nude mice (strain J:NU no. 7850 EC, Jackson Laboratories) were hydrodynamically transfected by injecting 20 µg of pcDNA3.1-CAG-luciferase plasmid DNA in 1.8 ml of 0.9% NaCl into the tail vein within 5–6 s. Animals were randomly assigned to receive AkaLuc, LumiScarlet, Antares or Antares2 plasmids. The person performing the tail vein injections was blinded as to the plasmids being injected. Then, 18 h after injection, mice were anesthetized with inhaled isoflurane via face mask for substrate injection and imaging. AkaLuc-expressing mice were injected i.p. with 3 µmol (1.0 mg) of AkaLumine-HCl (Sigma-Aldrich) in 100 µl 0.9% NaCl. Antares-expressing mice were injected i.p. with 4 µmol (1.6 mg) of compound B (HFz) in 480 µl of injectable formulation containing 10% ethanol (v/v), 10%/8% glycerol(v/v), 10% 2-hydroxypropyl-β-cyclodextrin (HPBCD, w/v) and 35% PEG-300/PEG-400 (v/v) in water, or with 1.3 µmol (0.56 mg) of compound F (FFz) in 150 µl of 12 mg poloxamer-407 in water. Antares2-expressing mice were injected i.p. with 1 µmol (0.4 mg) of DTZ in 480 µl of injectable formulation containing 10% ethanol (v/v), 10%/8% glycerol(v/v), 10% 2-Hydroxypropyl-β-cyclodextrin (HPBCD, w/v) and 35% PEG-300/PEG-400 (v/v) in water. LumiScarlet-expressing mice were injected i.p. with 4 µmol (1.5 mg) of 8pyDTZ in 480 µl of injectable formulation containing 10% ethanol (v/v), 10% glycerol(v/v), 10% 2-hydroxypropyl-β-cyclodextrin (HPBCD, w/v) and 35% PEG-300 (v/v) in water. Images were immediately acquired in the Ami HT optical imaging system every 1 min for 20 min. Imager settings were: emission filter, open; field of view, 25 cm; f-stop 1.2; binning, 1×1 and exposure time, 1 s. Images were analyzed as described above.

Long-term imaging of a bioluminescent calcium indicator. For calcium imaging, transgenic mice doubly hemizygous for *albumin-Cre* and *CAG-LSL-Orange CaMBI 110* with abdominal hair removed were anesthesized by i.p. injection of ketamine at 200 mg kg^{-1} in 100 µl water. After sedation, mice were injected with HFz and poloxamer-407 dissolved in 480 µl water, then placed in a lab-built imaging system. The imaging system was composed of a 15×15×15-inch black particle board cabinet with a hinged door (Foremost 327506). Strips of black padding were adhered along the door edges to create a light-tight seal on door closure. A circular opening with a diameter of 56 mm in the top panel was created using a circular saw, then a mirrorless interchangeable-lens digital camera (Olympus OM-D EM-5 Mark II) with a 25-mm f/1.7 lens (Panasonic H-H05) was mounted by inserting the front ring of the lens snugly into the opening. Images were acquired with exposure time of 1 s and aperture of f/1.7 in monotone picture mode, using the time-lapse function at a rate of one frame per 4.5 s. Files were saved in Olympus raw format onto a UHS-II-specification memory card (Lexar LSD64GCRBNA2000R), converted to 16-bit TIFF using the Olympus Viewer 3 program for Macintosh and analyzed using Fiji.

Bioluminescence imaging of subcutaneously implanted cells. For imaging subcutaneously implanted cells, HeLa cells or EW8 cells stably expressing luciferases were dissociated with trypsin and resuspended in DMEM and then changed to PBS. To count 1,000 cells, cells were collected from a FACSJazz cell sorter. The collected 1,000 cells were resuspended in 100 µl FBS-free DMEM containing 50% Matrigel matrix (Corning). First, 8-week-old male nude mice were anesthetized using isoflurane. Cells were subcutaneously injected into the left thoracolumbar regions. Mice were recovered on heat pads for 30 min while cells were allowed to settle. At 3 h posttumor implants, mice were i.p. injected with either 1.3 µmol (0.56 mg) of compound F (FFz) in 150 µl of injectable formulation containing 12 mg poloxamer-407 in water or 3 µmol (1.0 mg) of AkaLumine-HCl (Sigma-Aldrich) in 100 µl 0.9% NaCl for imaging. At 21 h posttumor implants, the same cohort of mice were i.p. injected with the other luciferin for imaging. Immediately after luciferin administration images were acquired in the Ami HT optical imaging system every 1 min for 20 min. Imager settings were: emission filter, open; field of view, 25 cm; f-stop 1.2; binning, 2×2 and exposure time, 60 s. Images were analyzed as described above.

Dual bioluminescence imaging of tumor and CAR-T cells. For dual imaging of engrafted tumors and CAR-T cells, EW8 cells or MG63.3 cells stably expressing luciferases were dissociated with trypsin and resuspended in RPMI and then changed to PBS. Cell numbers were determined using a hemocytometer and cell viability was determined using a trypan blue exclusion test. Then, 10^5 cells were resuspended in 100 µl PBS. Cells were intramuscularly injected into the thigh muscles of the hind limb of 8-week-old male nod scid (strain Nod scid no. 001303, Jackson Laboratories) or NSG mice (strain NSG no. 005557, Jackson Laboratories). For studying CAR-T cells-mediated tumor recession, 1.25 million B7-H3 or mock CAR-T cells expressing luciferases were intravenously injected into the tumor-grafted NSG mice 14 d posttumor implants. To image the luciferase-expressing cells, on indicated days posttumor implants, mice were i.p. injected with either 1.3 µmol (0.56 mg) of compound F (FFz) in 150 µl of injectable formulation containing 12 mg poloxamer-407 in water or 3 µmol (1.0 mg) of AkaLumine-HCl (Sigma-Aldrich) in 100 µl 0.9% NaCl for imaging. Immediately after luciferin administration images were acquired in the Ami HT optical imaging system every 1 min for 10 min. Image settings for tumor cells were f-stop 1.2, binning 2 and exposure time 1 s. Image settings for T cells were f-stop 1.2, binning 2 and exposure time 30 s. Images were analyzed as described above.

Animal procedures were performed in compliance with USDA and NIH ethical regulations and approved by the Stanford Institutional Animal Care and Use Committee.

Necropsy and histopathology. Male C57Bl/6 mice of 4 months of age were euthanized by CO_2 asphyxiation and cardiac exsanguination. Terminal cardiac blood was collected for complete blood counts and serum biochemistry. All mice were weighed and a complete gross examination of the external and internal organs was performed. The following tissues were collected and immersion-fixed in 10% neutral-buffered formalin for 72 h: liver, kidneys and lung. Formalin-fixed tissues were processed routinely, embedded in paraffin, sectioned at 5 µm and stained with hematoxylin and eosin. All slides were blindly evaluated for histologic treatment-related effects (Supplementary Table 3) by a board-certified veterinary pathologist.

Statistics. In animal bioluminescence experiments, variance was assessed in a sample of three mice, then the number of replicates (defined as individual mice) needed to detect an effect size with an alpha level of 0.05 was calculated using the program G*Power. For comparison of bioluminescence between two groups, normality of data was verified with the Shapiro–Wilk test, then a two-tailed Student's *t*-test was performed in Graphpad Prism 8. For comparison between

three groups, normality of data was verified with the Shapiro–Wilk test, then one-way analysis of variance with Tukey's posthoc test was performed in Graphpad Prism 8.

Reporting Summary. Further information on research design is available in the Nature Research Reporting Summary linked to this article.

Data availability

The data that support the findings of this study are available from the corresponding authors upon request.

References

29. Shakhmin, A. et al. Three efficient methods for preparation of coelenterazine analogues. *Chemistry* **22**, 10369–10375 (2016).
30. Shrestha, T., Troyer, D. & Bossmann, S. Strategies for large-scale synthesis of coelenterazine for in vivo applications. *Synthesis* **46**, 646–652 (2014).
31. Walker, A. J. et al. Tumor antigen and receptor densities regulate efficacy of a chimeric antigen receptor targeting anaplastic lymphoma kinase. *Mol. Ther.* **25**, 2189–2201 (2017).
32. Schindelin, J. et al. Fiji: an open-source platform for biological-image analysis. *Nat. Methods* **9**, 676–682 (2012).

Acknowledgements

We thank H. Zeng and the Stanford Transgenic, Knockout, and Tumor Model Center for generating *H11P-CAG-LSL-Antares* and *-FLuc* transgenic mice, C. Manalac and L. Luo (Stanford University) for *nestin-Cre* transgenic mice, and G. Tao and K. Sylvester (Stanford University) for *albumin-Cre* transgenic mice. We thank J. Osterman and H. Lazaro in the analytical department at Promega Biosciences for their support in compound characterization. Cell sorting/flow cytometry analysis for this project was done on instruments in the Stanford Shared FACS Facility. We thank the Stanford Animal Histology Services for help with preparation of histologic specimens. This work was supported by American Heart Association Innovative Research grant no. 15IRG23290018 (M.Z.L.), NIH grant no. 1R21DA048252 (M.Z.L.), an American Heart Association Postdoctoral Fellowship (N.K.), NCI grant no. P5P30CA124435 (C.L.M.), a St Baldrick's/Stand Up 2 Cancer Pediatric Dream Team Translational Cancer Research Grant (C.L.M.), Virginia and D.K. Ludwig Fund for Cancer Research (C.L.M.) and Stanford University School of Medicine Discovery Innovation Awards (J.R.C. and M.Z.L.). Stand Up 2 Cancer is a program of the Entertainment Industry Foundation administered by the American Association for Cancer Research. C.L.M is a member of the Parker Institute for Cancer Immunotherapy, which supports the Stanford University Cancer Immunotherapy Program. L.L. received support from the National Science Foundation Graduate Research Fellowship, Stanford Graduate Fellowship and Stanford EDGE Fellowship. R.G.M. is the Taube Distinguished Scholar for Pediatric Immunotherapy at Stanford University School of Medicine.

Author contributions

Y.S. performed mouse experiments, analyzed data, prepared figures and wrote the manuscript. J.R.W. designed and synthesized new substrates. Y.P. performed solubility and mouse experiments, analyzed data and prepared figures. T.P.S. designed and prepared extended-release formulations. D.C.W. assisted with mouse experiments and created the FLuc integration plasmid. M.P.H. performed biochemical assays and prepared figures. L.X.L. performed mouse breeding and genotyping. R.H. assisted with protein purifications. L.P.E. assisted with cloning and protein expression. L.L. generated retroviral supernatants and prepared engineered T cells and tumor cells. N.K. created the Antares integration plasmid. K.M.C. performed mouse histopathology and prepared figures. F.Z. performed hydrodynamic transfection in mice. R.G.M., J.R.C., C.L.M. and M.A.K. provided supervision. T.A.K. designed experiments and provided supervision. M.Z.L. conceived the project, provided supervision, designed experiments, prepared figures and wrote the manuscript.

Competing interests

J.R.W., T.P.S., M.P.H., R.H., L.P.E. and T.A.K. are employees of Promega Corporation and inventors on a patent describing furimazine and furimazine derivatives. L.L. is a consultant for Lyell Immunopharma. R.G.M. is a consultant for Lyell Immunopharma, Xyphos Biosciences, Gamma Delta Therapeutics and Illumina Radiopharmaceuticals. Y.P., D.C.W., L.X.L., Y.S., N.K., K.M.C. and M.Z.L. declare no competing interests. C.L.M. is a founder, holds equity in and is a consultant for Lyell Immunopharma, consults for Neoimmune Tech, Apricity and Nektar, holds equity in Apricity and Allogene and has received royalties from NIH for a CD22-CAR licensed to Juno.

Additional information

Extended data is available for this paper at https://doi.org/10.1038/s41592-020-0889-6.

Supplementary information is available for this paper at https://doi.org/10.1038/s41592-020-0889-6.

Correspondence and requests for materials should be addressed to T.A.K. or M.Z.L.

Peer review information Rita Strack was the primary editor on this article and managed its editorial process and peer review in collaboration with the rest of the editorial team.

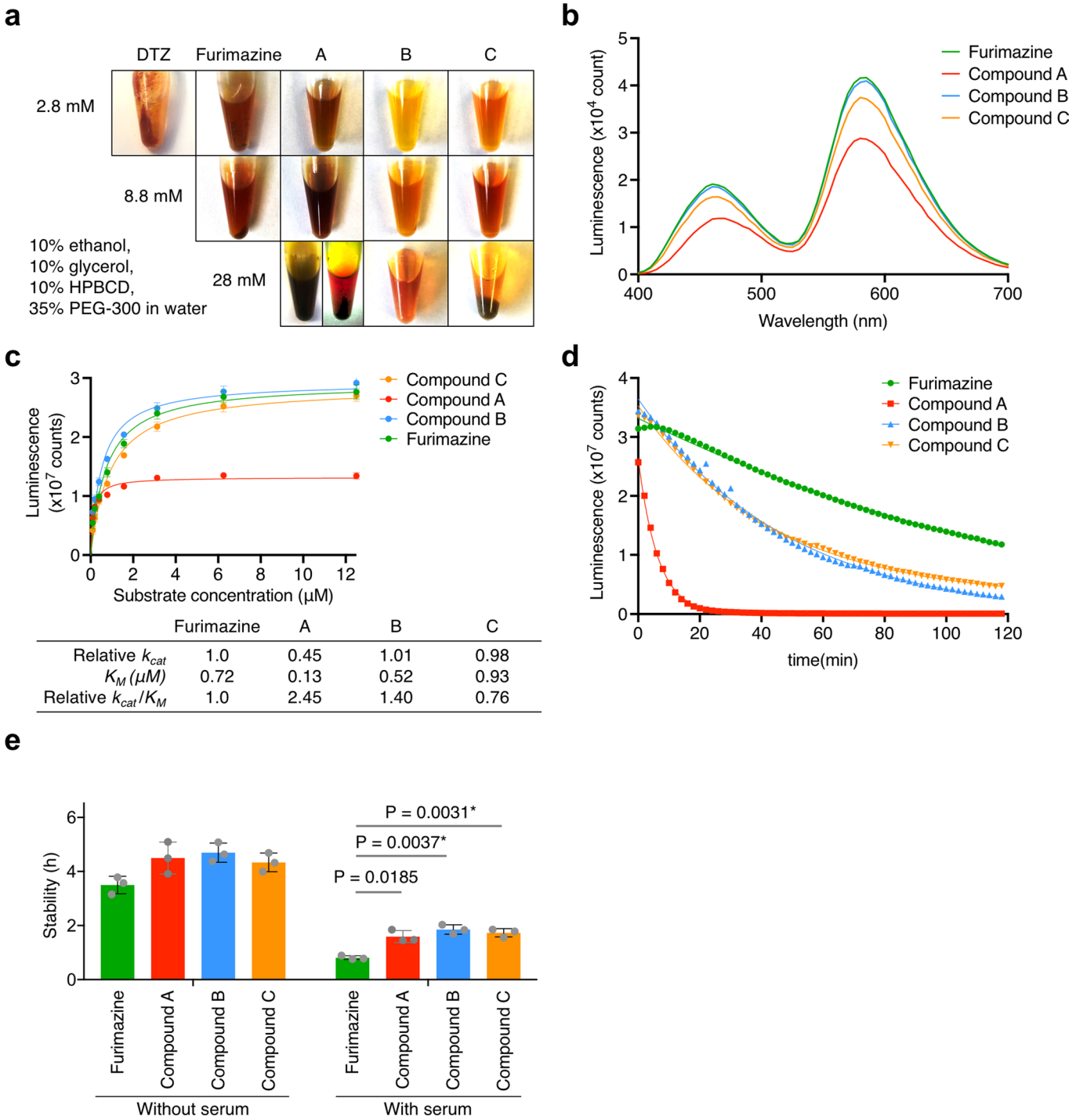

	Furimazine	A	B	C
Relative k_{cat}	1.0	0.45	1.01	0.98
K_M (μM)	0.72	0.13	0.52	0.93
Relative k_{cat}/K_M	1.0	2.45	1.40	0.76

Extended Data Fig. 1 | *In vitro* characterization of novel furimazine analogs. a, Solubility of furimazine analogs at various concentrations in 35% PEG-300, 10% ethanol, 10% glycerol and 10% hydroxypropylcyclodextrin. Images were taken in ambient light, except for the right image of compound A at 28 mM, which was taken under backlit conditions to more clearly show an insoluble pellet. The experiment was repeated independently two times with similar results. **b**, Spectral profiles of Antares with furimazine and analogues. The experiment was repeated independently two times with similar results. **c**, Determination of kinetic parameters of relative k_{cat} and absolute K_M for Antares with each substrate. As the same concentration of purified Antares was used with each substrate, k_{cat} relative to furimazine can be calculated from the relative asymptotic luminescence (V_{max}) values. Error bars, standard error of the mean (s.e.m.). N = 3. **d**, Decay of signal over time of Antares signal with furimazine substrates. The experiment was repeated independently two times with similar results. **e**, Stability of furimazine substrates at 37 °C in the presence and absence of 10% FBS. Colored bars, mean of three biological replicates. Gray dots, individual values. Error bars, standard error of the mean (s.e.m.). P values, ordinary one-way ANOVA or two-tailed Student's t test.

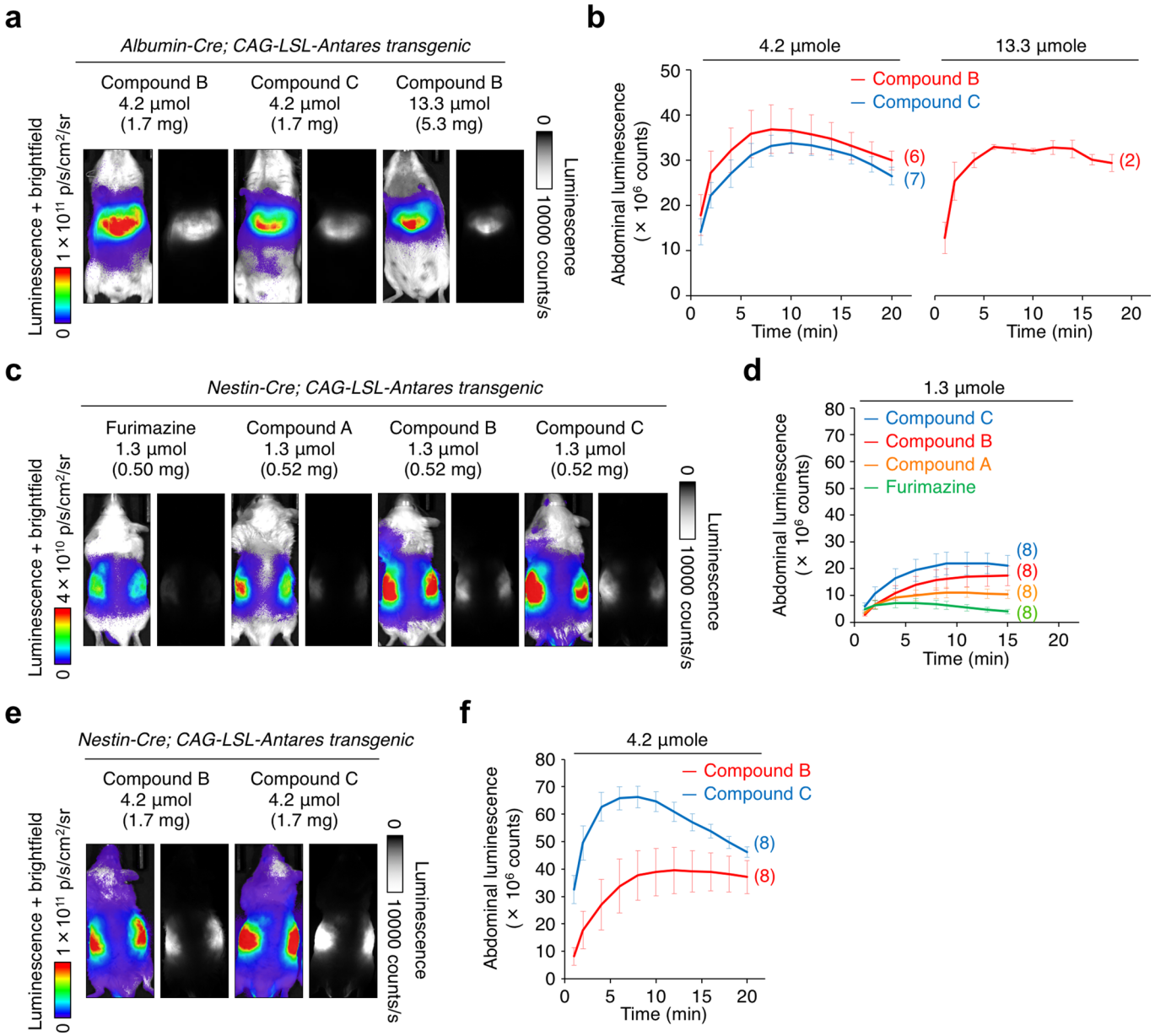

Extended Data Fig. 2 | Comparing *in vivo* brightness of Antares with furimazine to new substrates. Bioluminescence imaging was performed in mice doubly hemizygous for *Albumine-cre* **a-b**, *or nestin-Cre* **c-f**, and *CAG-loxP-stop-loxP-Antares* (*CAG-LSL-Antares*) genes, which express Antares protein in the liver or kidney. For liver imaging (**a-b**), 4.2 µmol or 13.3 µmol of each substrate was injected intraperitoneally (**a**), with quantitation of the mean bioluminescence intensity over time shown (**b**). Similarly, for kidney imaging (**c-f**), 1.3 µmol (**c-d**) or 13.3 µmol (**e-f**) of each substrate was injected intraperitoneally. Exposure = 1 s, Binning = 1, Fstop = 8. Error bars, standard error of the mean (s.e.m.). Numbers of mice are indicated in parentheses.

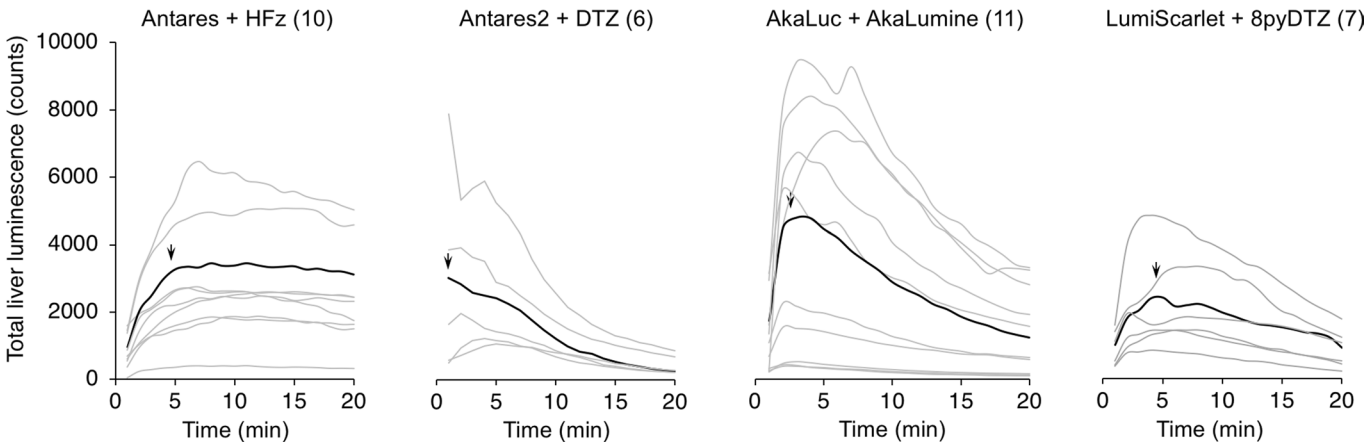

Extended Data Fig. 3 | Individual bioluminescence traces of luciferase–luciferin pairs in deep tissues of live mice. Traces of total bioluminescence intensity in the liver for each hydrodynamically transfected mouse in the groups of Antares + compound B (n = 10), Antares2 + DTZ (n = 6), and AkaLuc + AkaLumine (n = 11) were displayed in gray. The bioluminescence trace of selected mouse shown in Fig. 2a was plotted in black curve. Arrows indicate the time points of displayed images in Fig. 2a.

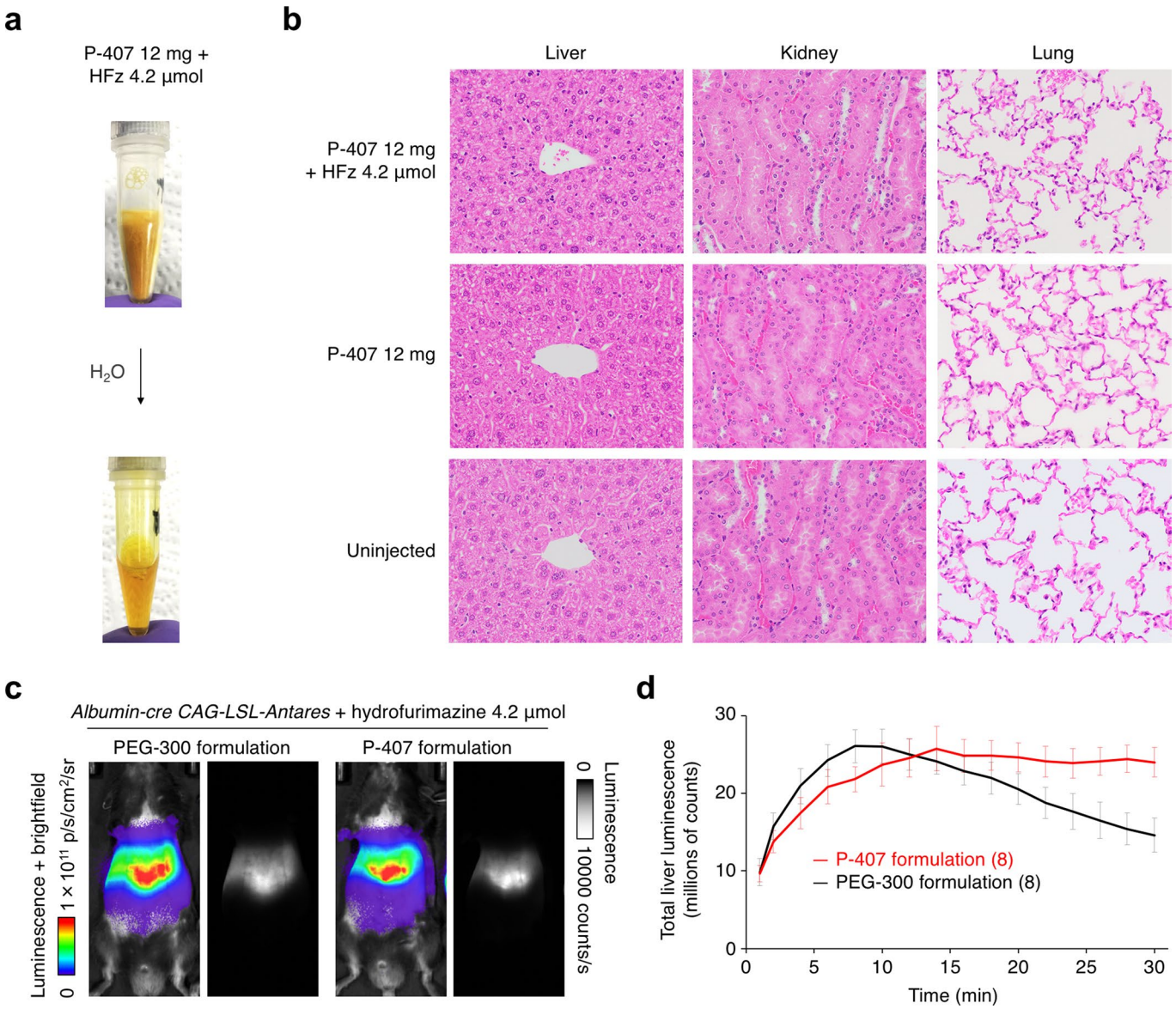

Extended Data Fig. 4 | Characterization of compound B in a P-407-based formulation. a, 4.2 µmol (1.7 mg) of compound B and 11.1 mg P-407 can be dissolved in ethanol, evaporated, redissolved in water, and lyophilized to create a lyophilized cake (top). 480 µL of water can then be added to resolubilize the compound B and P-407 (bottom). **b**, Sections of lung, liver, and kidney show no signs of toxicity following administration of P-407 or compound B with P-407. Mice received three daily intraperitoneal injections of 12 mg P-407 in 480 µL of water or of 1.7 mg compound B and 12 mg P-407 in 480 µL of water, then were sacrificed on the fourth day. Organs were fixed in formalin, embedded in paraffin, sectioned, de-paraffinized, and stained with hematoxylin and eosin. **c**, Comparison of bioluminescence intensity and persistence *in vivo* between the published PEG-300-based formulation and a poloxamer-407-based extended-release formulation of HFz (compound B). **d**, Mean bioluminescence intensity over time for the injected formulations. Error bars, standard error of the mean (s.e.m.). Numbers of mice are indicated in parentheses.

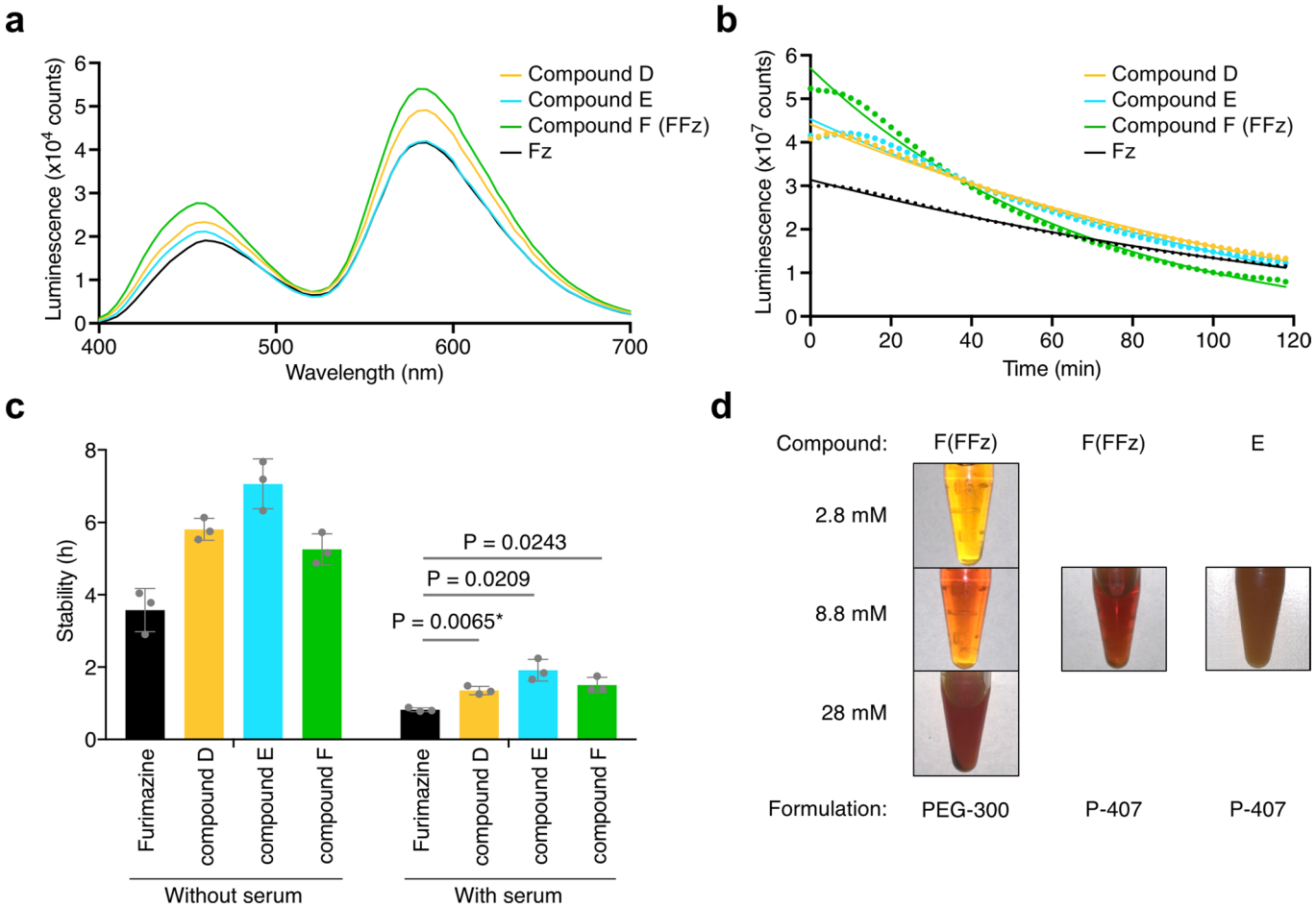

Extended Data Fig. 5 | *In vitro* characterization of novel fluorinated furimazine analogs. a, Spectral profiles of Antares with fluorinated furimazine analogues. The experiment was repeated independently two times with similar results. **b**, Decay of signal over time of Antares signal with furimazine substrates. The experiment was repeated independently two times with similar results. **c**, Stability of furimazine substrates at 37 °C in the presence and absence of 10% FBS. Colored bars, mean of three biological replicates. Gray dots, individual values. Error bars, standard error of the mean (s.e.m.). P values, ordinary one-way ANOVA or two-tailed Student's t test. **d**, Solubility of fluorinated furimazine analogs at various concentrations in an aqueous formulation containing 35% PEG-300, 10% ethanol, 10% glycerol and 10% hydroxypropylcyclodextrin, or a formulation containing 12 mg P-407 in 0.5 mL water. The experiment was repeated independently two times with similar results.

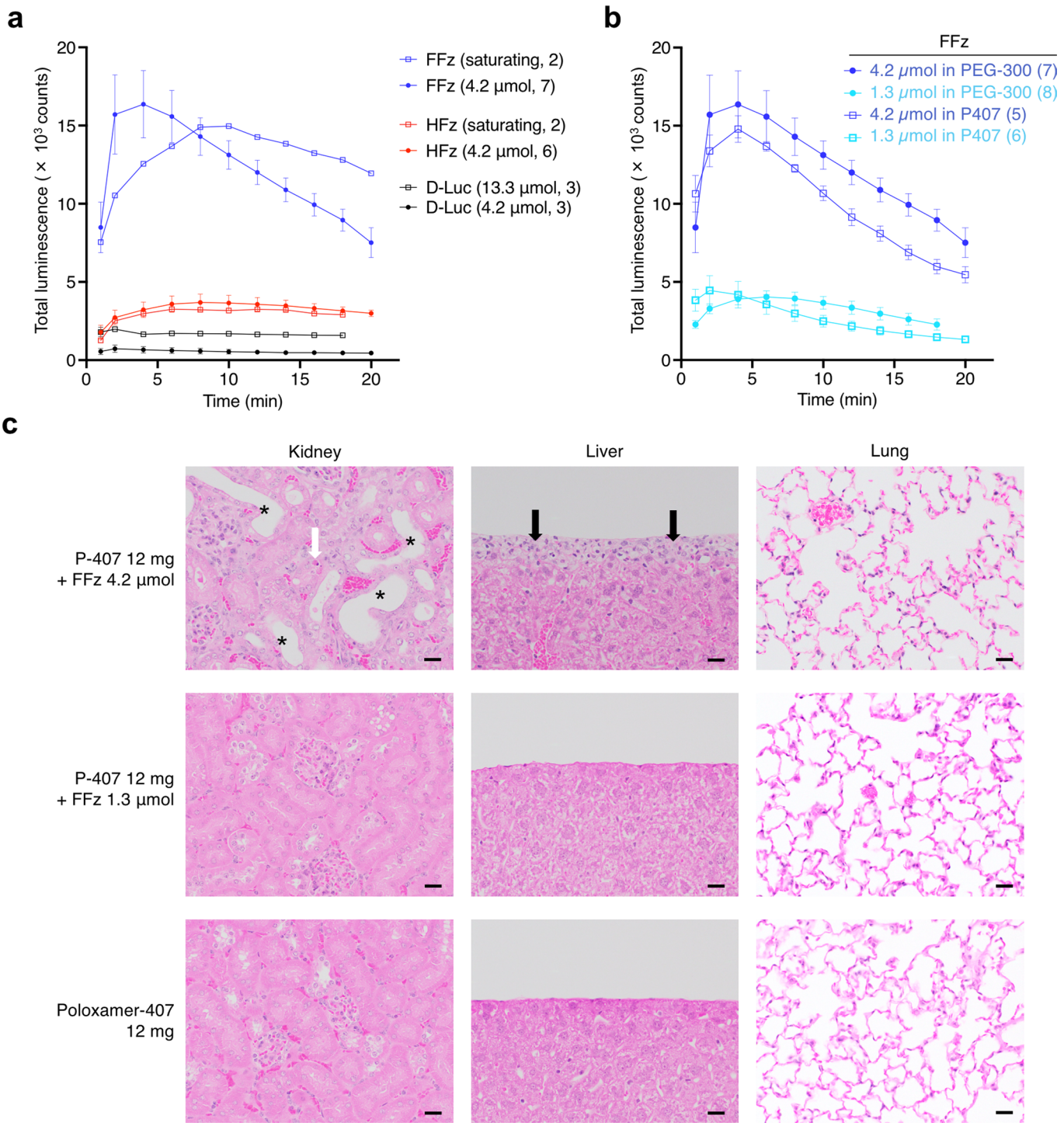

Extended Data Fig. 6 | Establishing optimal dosage and vehicle for FFz administration in mice. a, Mean bioluminescence intensity over time for bioluminescence imaging results in mice doubly hemizygous for *albumin-Cre* and *CAG-loxP-stop-loxP-Antares or luc2* (*CAG-LSL-Antares or FLuc*) genes, which express Antares or FLuc protein in the liver, and injected with indicated amount of luciferins to establish saturating dosage for each luciferin **b**, Mean bioluminescence intensity over time for comparing the effects of formulation on fluorofurimazine (FFz). Error bars, standard error of the mean (s.e.m.). Numbers of mice are indicated in parentheses. **c**, Renal and hepatic histologic lesions are most severe in mice receiving FFz (4.2 µmol) following 3 days of intraperitoneal administration. Mice receiving FFz (4.2 µmol) exhibited renal tubular degeneration (white arrow), renal tubular dilation (asterisks), and hepatic capsular degeneration with neutrophilic infiltrates (black arrows). Renal and hepatic lesions were minimal to absent in mice receiving compound FFz (1.3 µmol) or vehicle (P407) alone. No lesions were noted in the lungs across any groups. Hematoxylin and eosin, scale bar = 20 µm. The experiment was repeated independently three times with similar results.

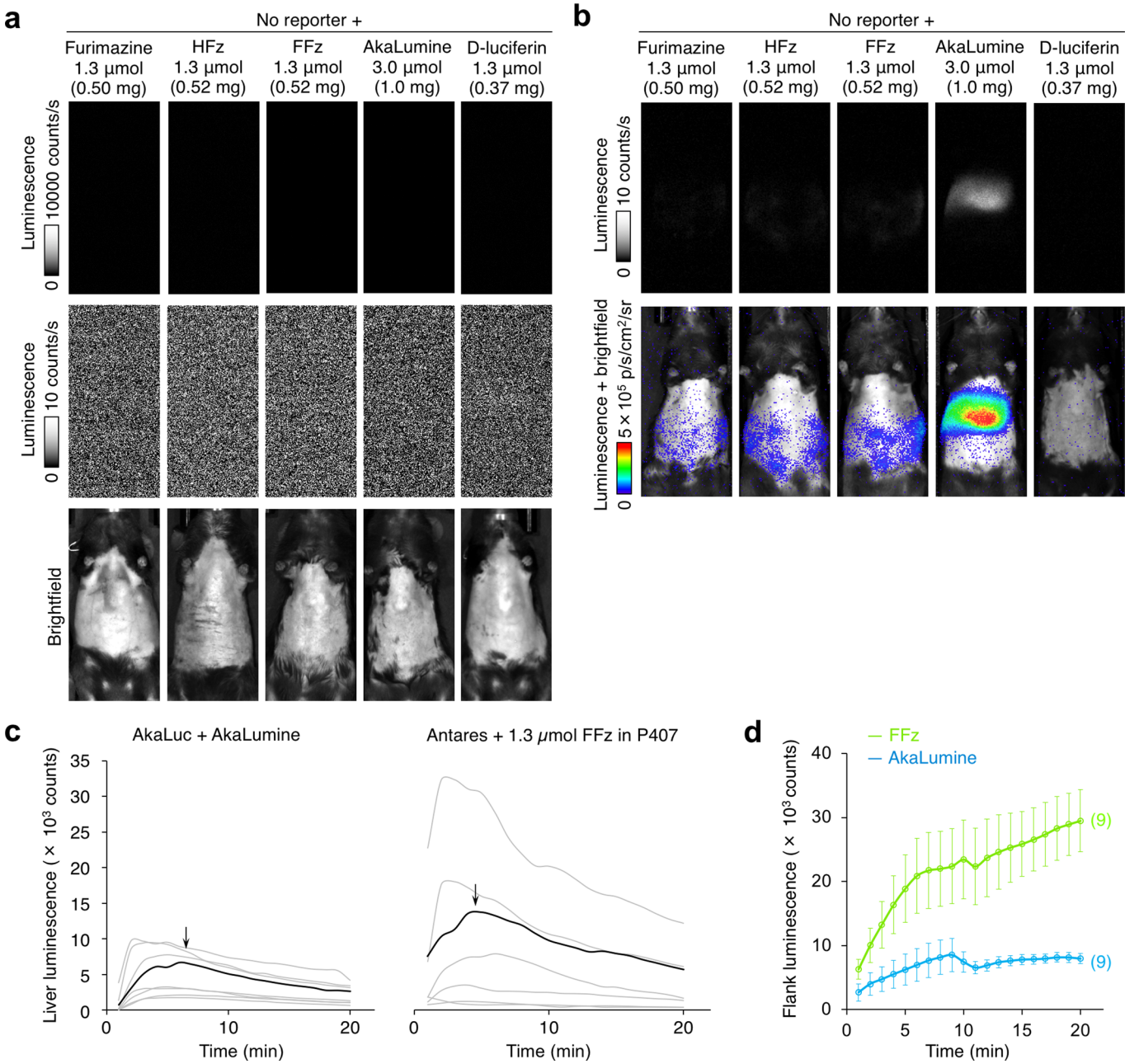

Extended Data Fig. 7 | Details of background and signal comparisons. To assess background luminescence for furimazine, HFz, FFz, AkaLumine, or D-luciferin mice lacking any luciferase genes were injected with the indicated amounts of substrates. **a**, No luminescence was observed for all the luciferase substrates at the low sensitivity settings (Exposure = 1 s, Binning = 1, Fstop = 8). The experiment was repeated independently two times with similar results. **b**, Under the high sensitivity imaging settings (Exposure = 60 s, Binning = 2, Fstop = 1.2), no significant luminescence except for the occasional signal at the injection site was observed for all the mice injected with furimazine analogues, while liver signal were observed with AkaLumine injected. The experiment was repeated independently two times with similar results. **c**, Traces of total bioluminescence intensity in the liver for each hydrodynamically transfected mouse in the groups of AkaLuc + AkaLumine (n = 8) and Antares + FFz (n = 7) were displayed in gray. The bioluminescence trace of selected mouse shown in Fig. 4a was plotted in black curve. Arrows indicate the time points of displayed images in Fig. 4a. **d**, Mean signal intensity over time from 10^3 HeLa[Antares-P2A-AkaLuc] cells implanted subcutaneously after injection of FFz or AkaLumine. Note the slower kinetics compared to bioluminescence time courses in the liver. This can be explained by lack of vascularization of the implanted HeLa cells, which were imaged within 24 h of implantation. Note AkaLumine signals have reached a plateau whereas FFz signals have not at 20 min, so the peak and integrated signals of FFz relative to AkaLumine are likely underestimated. Error bars, standard error of the mean (s.e.m.). Numbers of mice are indicated in parentheses.

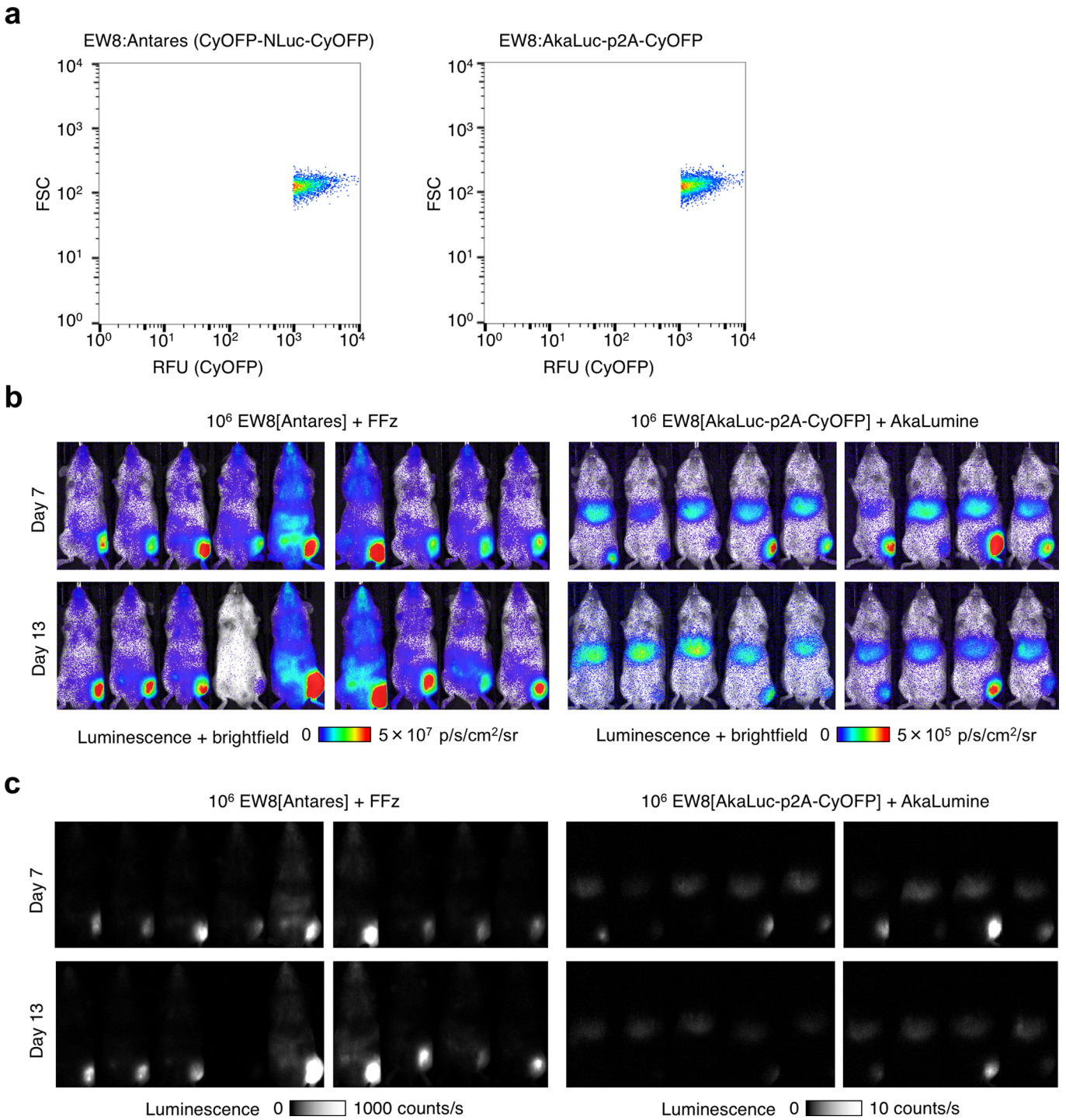

Extended Data Fig. 8 | Bioluminescence imaging engrafted luciferase-expressing EW8 tumors in nod scid mice. a, Flow cytometry characterization of EW8 cells stably expressing indicated luciferase. Wild-type EW8 cells were lentiviral transduced with indicated constructs, expanded, and then sorted based on CyOFP reporter fluorescence. The experiment was repeated independently two times with similar results. **b**, Bioluminescence imaging in nod scid mice engrafted with luciferase-expressing EW8 tumors in one leg (at day 0). 1.3 µmol FFz (0.15 mL in P-407) or 1.5 µmol AkaLumine (0.10 mL in 0.9% saline) were injected IP on the indicated days. **c**, Raw grayscale images. Imager settings: Exposure time = 2 s (FFz) or 60 s (AkaLumine), Binning = 2, Fstop = 1.2.

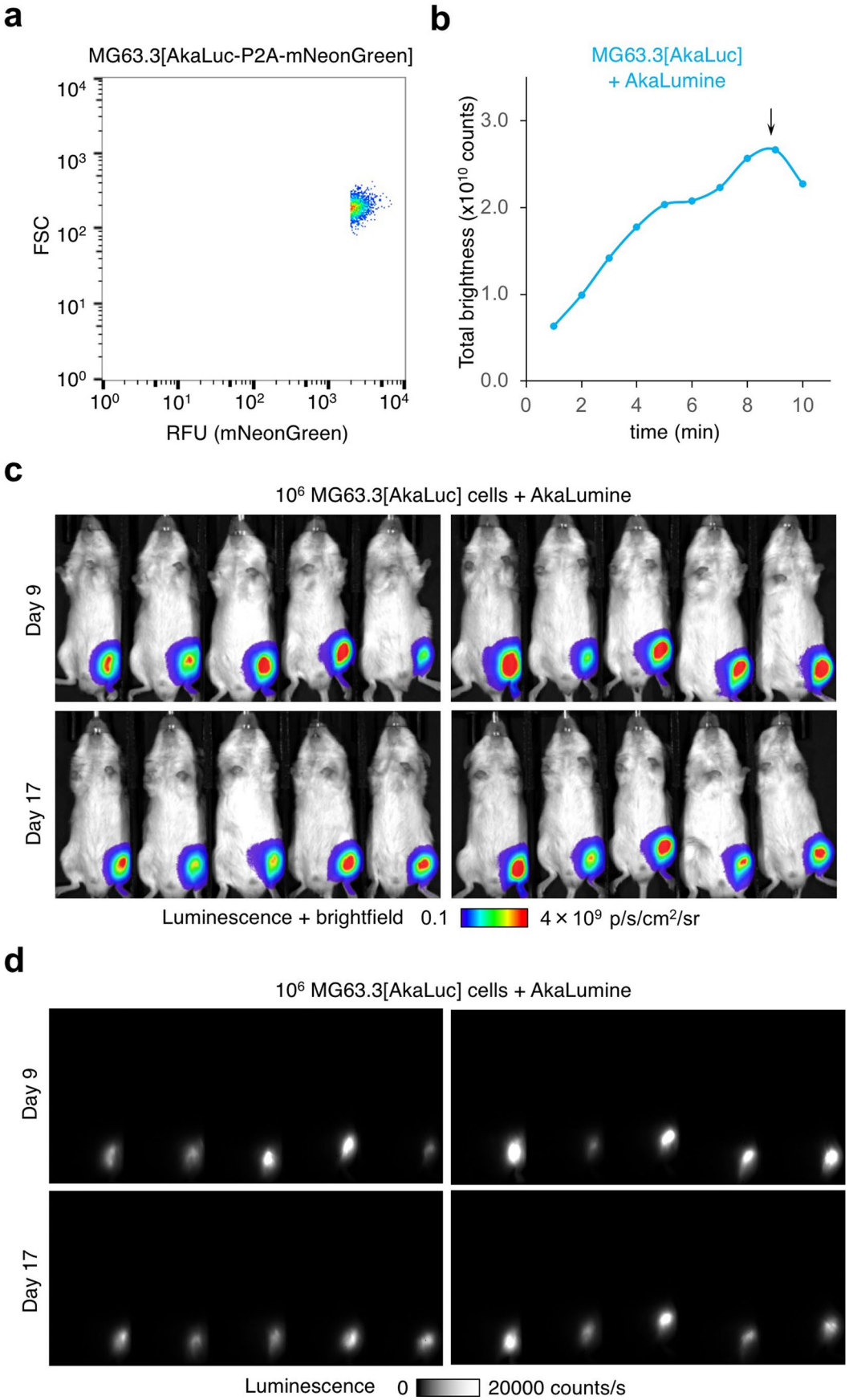

Extended Data Fig. 9 | See next page for caption.

Extended Data Fig. 9 | Bioluminescence imaging engrafted AkaLuc-expressing MG63.3 tumors in NSG mice. a, Flow cytometry characterization of MG63.3 cells stably expressing AkaLuc-p2A-mNeonGreen. Wild-type MG63.3 cells were retroviral transduced with indicated constructs, expanded, and then sorted based on mNeonGreen reporter fluorescence. The experiment was repeated independently two times with similar results. **b**, Representative *in vivo* bioluminescence time course from grafted AkaLuc-expressing MG63.3 tumor after AkaLumine injection. Arrow indicates time point used for quantitation. The experiment was repeated independently ten times with similar results. **c**, Bioluminescence imaging in NSG mice engrafted with AkaLuc-expressing MG63.3 tumors in one leg (at day 0). 3.0 μmol AkaLumine (0.10 mL in 0.9% saline) were injected IP on the indicated days. **d**, Raw grayscale images. Imager settings: Exposure time = 1 s, Binning = 1, Fstop = 1.2.

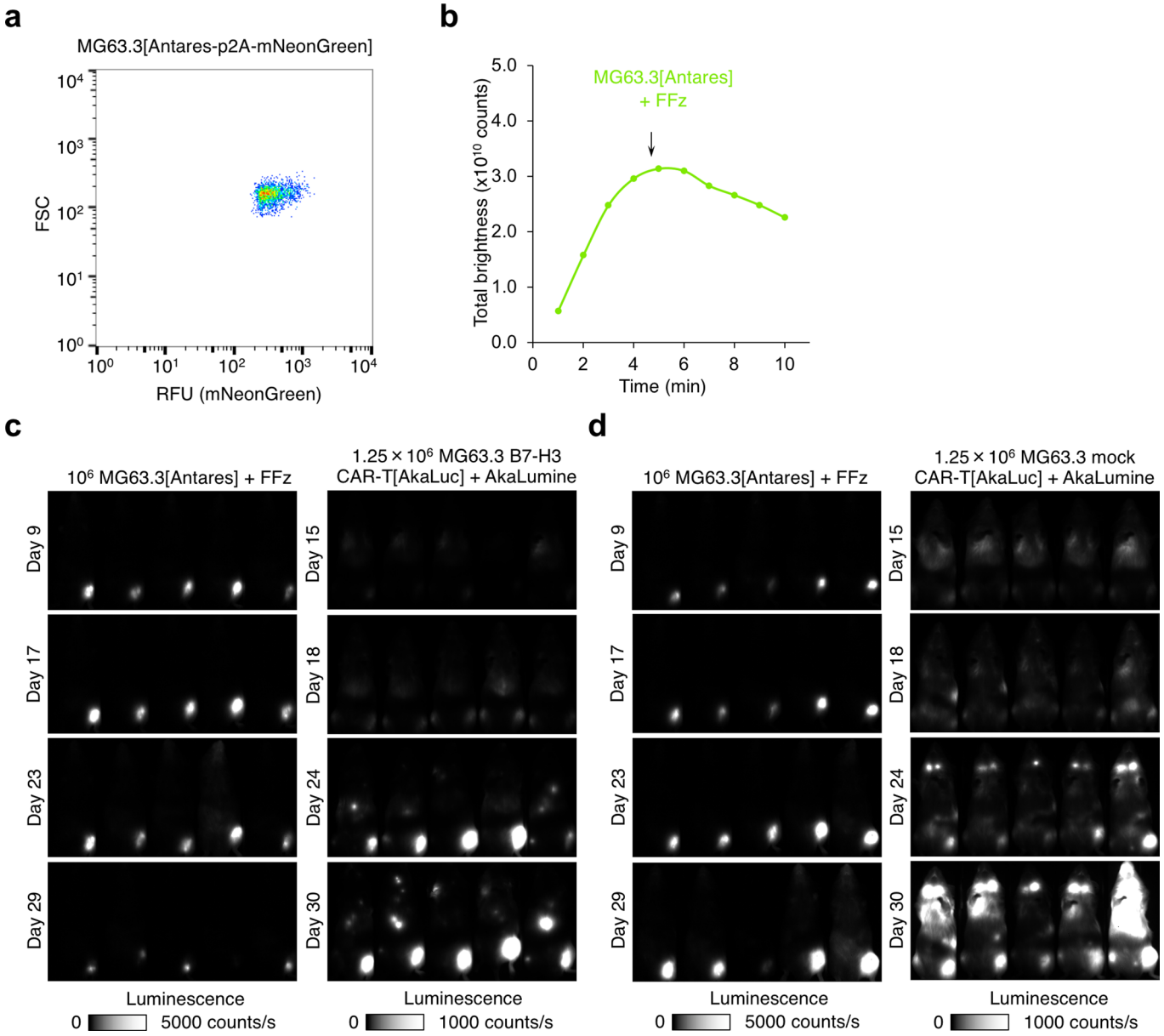

Extended Data Fig. 10 | Dual bioluminescence imaging MG63.3 tumors and non-immune T cells in NSG mice. a, Flow cytometry characterization of MG63.3 cells stably expressing Anatares-p2A-mNeonGreen. Wild-type MG63.3 cells were retroviral transduced with indicated constructs, expanded, and then sorted based on mNeonGreen reporter fluorescence. The experiment was repeated independently two times with similar results. **b**, Representative *in vivo* bioluminescence time course from grafted Antares-expressing MG63.3 tumors after FFz injection. Arrow indicates timepoint used for quantitation. The experiment was repeated independently ten times with similar results. **c-d**, Raw grayscale images of NSG mice engrafted with Antares-expressing MG63.3 tumors in one leg (at day 0) and intravenously injected with AkaLuc-expressing cells (**d**) B7-H3 CAR-T (Fig. 5a) or (**e**) mock CAR-T (native T) cells (Fig. 5b).

nature research

Corresponding author(s): Lin MZ and Kirkland TA

Last updated by author(s): Apr 8, 2020

Reporting Summary

Nature Research wishes to improve the reproducibility of the work that we publish. This form provides structure for consistency and transparency in reporting. For further information on Nature Research policies, see Authors & Referees and the Editorial Policy Checklist.

Statistics

For all statistical analyses, confirm that the following items are present in the figure legend, table legend, main text, or Methods section.

n/a	Confirmed	
☐	☒	The exact sample size (*n*) for each experimental group/condition, given as a discrete number and unit of measurement
☐	☒	A statement on whether measurements were taken from distinct samples or whether the same sample was measured repeatedly
☐	☒	The statistical test(s) used AND whether they are one- or two-sided *Only common tests should be described solely by name; describe more complex techniques in the Methods section.*
☒	☐	A description of all covariates tested
☐	☒	A description of any assumptions or corrections, such as tests of normality and adjustment for multiple comparisons
☐	☒	A full description of the statistical parameters including central tendency (e.g. means) or other basic estimates (e.g. regression coefficient) AND variation (e.g. standard deviation) or associated estimates of uncertainty (e.g. confidence intervals)
☐	☒	For null hypothesis testing, the test statistic (e.g. *F*, *t*, *r*) with confidence intervals, effect sizes, degrees of freedom and *P* value noted *Give P values as exact values whenever suitable.*
☒	☐	For Bayesian analysis, information on the choice of priors and Markov chain Monte Carlo settings
☒	☐	For hierarchical and complex designs, identification of the appropriate level for tests and full reporting of outcomes
☒	☐	Estimates of effect sizes (e.g. Cohen's *d*, Pearson's *r*), indicating how they were calculated

Our web collection on statistics for biologists contains articles on many of the points above.

Software and code

Policy information about availability of computer code

Data collection	ImageJ, version:2.0.0; BD FACS Sortware, version 1.x; Ami Aura, version 2.2.1.1
Data analysis	ImageJ, version:2.0.0; Microsoft Excel, version:16.16.10 ; GraphPad Prism, version 8.0c; Ami Aura, version 2.2.1.1; FlowJo, version OSX10.6; Olympus Viewer 3, version 2.4.1

For manuscripts utilizing custom algorithms or software that are central to the research but not yet described in published literature, software must be made available to editors/reviewers. We strongly encourage code deposition in a community repository (e.g. GitHub). See the Nature Research guidelines for submitting code & software for further information.

Data

Policy information about availability of data

All manuscripts must include a data availability statement. This statement should provide the following information, where applicable:

- Accession codes, unique identifiers, or web links for publicly available datasets
- A list of figures that have associated raw data
- A description of any restrictions on data availability

The data that support the findings of this study are available from the corresponding authors upon request.

Field-specific reporting

Please select the one below that is the best fit for your research. If you are not sure, read the appropriate sections before making your selection.

☒ Life sciences ☐ Behavioural & social sciences ☐ Ecological, evolutionary & environmental sciences

Life sciences study design

All studies must disclose on these points even when the disclosure is negative.

Sample size	To test for differences in peak brightness, signal durability, and integrated output between luciferase-substrate system in mice, a power analysis was first performed in the program G*Power to determine that a sample size of 8 was needed to detect an effect size of 2 given expected coefficients of variation of 0.5. These effect sizes and coefficients of variation are similar to those previously observed in comparisons of bioluminescence systems [Nature biotechnology 34, 760 (2016).]
Data exclusions	In the experiment of comparing luciferase-luciferin pairs in hydrodynamic transfected nude mice, some data were excluded due to errors in substrate injection practice (wrong area for IP injection). The exclusion criteria were not pre-established.
Replication	All findings were replicatable across multiple preparations. All the data presented were repeated independently at least two times to verify the reproducibility of the experimental findings.
Randomization	All experimental conditions used a common set of starting materials and were performed in parallel. Individual animals from the same strain were randomly selected for injecting different substrate and/or imaging.
Blinding	Hydrodynamic transfection of plasmids was performed blindly. Other experimenters and analysis could not be blinded during data collection as appropriate filters had to be selected for each construct.

Reporting for specific materials, systems and methods

We require information from authors about some types of materials, experimental systems and methods used in many studies. Here, indicate whether each material, system or method listed is relevant to your study. If you are not sure if a list item applies to your research, read the appropriate section before selecting a response.

Materials & experimental systems

n/a	Involved in the study
☒	☐ Antibodies
☐	☒ Eukaryotic cell lines
☒	☐ Palaeontology
☐	☒ Animals and other organisms
☐	☒ Human research participants
☒	☐ Clinical data

Methods

n/a	Involved in the study
☒	☐ ChIP-seq
☐	☒ Flow cytometry
☒	☐ MRI-based neuroimaging

Eukaryotic cell lines

Policy information about cell lines

Cell line source(s)	HeLa from ATCC, EW8 by L. Helman (NCI, NIH, Bethesda, MD), MG63.3 by C. Khanna (NCI, NIH, Bethesda, MD),
Authentication	None of the cell lines used were authenticated
Mycoplasma contamination	The HeLa cell lines were not tested with mycoplasma contamination. EW8 and MG63.3 cell lines were tested negative for mycoplasma contamination and have been cultured in a media with plasmocin
Commonly misidentified lines (See ICLAC register)	No commonly misidentified cell lines were used.

Animals and other organisms

Policy information about studies involving animals; ARRIVE guidelines recommended for reporting animal research

Laboratory animals	C57BL/6J mice, male and female, 6-16 weeks old; J:NU mice (#7850 EC, Jackson Laboratories), male, 7 weeks old; Nod scid mice (#001303, Jackson Laboratories), male, 7-8 weeks old; NSG mice strain NSG (#005557, Jackson Laboratories), male, 7-8 weeks old
Wild animals	This study doesn't involve wild animals
Field-collected samples	This study doesn't involve field-collected samples
Ethics oversight	The animal study is following a protocol approved by Administrative Panel on Laboratory Animal Care (APLAC), the IACUC at Stanford University

Note that full information on the approval of the study protocol must also be provided in the manuscript.

Human research participants

Policy information about studies involving human research participants

Population characteristics	Buffy coats from anonymous healthy (male and female human, ages 30-50) were purchased from the Stanford University Blood Bank.
Recruitment	Written informed consent was obtained from all healthy donors.
Ethics oversight	T cell isolation Healthy donor buffy coats were collected by and purchased from the Stanford Blood Center under an IRB-exempt protocol.

Note that full information on the approval of the study protocol must also be provided in the manuscript.

Flow Cytometry

Plots

Confirm that:

☒ The axis labels state the marker and fluorochrome used (e.g. CD4-FITC).

☒ The axis scales are clearly visible. Include numbers along axes only for bottom left plot of group (a 'group' is an analysis of identical markers).

☒ All plots are contour plots with outliers or pseudocolor plots.

☒ A numerical value for number of cells or percentage (with statistics) is provided.

Methodology

Sample preparation	Cultured cells were dissociated with trypsin and re-suspended in DMEM, and then changed to PBS.
Instrument	FACSJazz cell sorter (BD Biosciences)
Software	Flowjo, version OSX10.6
Cell population abundance	Top 5% brightest population based on the fluorescent marker were collected. Results of collected cell population were displayed in the manuscript.
Gating strategy	FSC/SSC gates to identify cells, FSC-A/Trigger pulse width to identify single cells, then corresponding fluorescence gates to profile the cells for sorting

☐ Tick this box to confirm that a figure exemplifying the gating strategy is provided in the Supplementary Information.